



## 1 **Parameterization of particle formation rates in distinct atmospheric environments**

2 Xinyang Li<sup>1,\*</sup>, Tuomo Nieminen<sup>1,2</sup>, Rima Baalbaki<sup>1,3</sup>, Putian Zhou<sup>1</sup>, Pauli Paasonen<sup>1</sup>, Risto Makkonen<sup>4</sup>, Martha A.  
3 Zaidan<sup>1,5</sup>, Nina Sarnela<sup>1</sup>, Chao Yan<sup>1,6</sup>, Tuija Jokinen<sup>1,3</sup>, Imre Salma<sup>7</sup>, Máté Vörösmarty<sup>8</sup>, Tuukka Petäjä<sup>1</sup>, Veli-Matti  
4 Kerminen<sup>1</sup>, Markku Kulmala<sup>1,6</sup>, Lubna Dada<sup>1,9,\*</sup>

5 <sup>1</sup> Institute for Atmospheric and Earth System Research (INAR), University of Helsinki, Helsinki, 00560, Finland

6 <sup>2</sup> Department of Physics, Faculty of Science, University of Helsinki, Helsinki, Finland

7 <sup>3</sup> Climate & Atmosphere Research Centre (CARE-C), Cyprus Institute, P.O. Box 27456, Nicosia, 1645, Cyprus

8 <sup>4</sup> Hevesy Climate System Research, Finnish Meteorological Institute, P.O. Box 503, 00101 Helsinki, Finland

9 <sup>5</sup> Department of Computer Science, University of Helsinki, Helsinki, 00560, Finland

10 <sup>6</sup> Joint International Research Laboratory of Atmospheric and Earth System Sciences, School of Atmospheric Sciences, Nanjing University,  
11 Nanjing, 210023, China

12 <sup>7</sup> Institute of Chemistry, Eötvös Loránd University, Budapest, Hungary

13 <sup>8</sup> Hevesy György Ph.D. School of Chemistry, Eötvös Loránd University, Budapest, Hungary

14 <sup>9</sup> PSI Center for Energy and Environmental Sciences, Villigen PSI, Switzerland

15 \*Correspondence to: Xinyang Li ([xinyang.li@helsinki.fi](mailto:xinyang.li@helsinki.fi)), Lubna Dada ([lubna.dada@helsinki.fi](mailto:lubna.dada@helsinki.fi))

16

17 **Abstract.** Atmospheric particle formation rate ( $J$ ) is one of the key characteristics in new particle formation (NPF)  
18 processes worldwide. It is related to the development of ultrafine particle growth to cloud condensation nuclei  
19 (CCN) and, hence, to Earth radiative forcing in global models, which helps us to better understand the impact of  
20 NPF on cloud properties and climate change. In this work, we parameterized four semi-empirical  $J$  models for 5  
21 nm atmospheric particles using field measurements obtained from distinct environments that varied from clean to  
22 heavily polluted regions and from tropical to polar regions. The models rely primarily on sulfuric acid as a  
23 condensing vapor, condensation sink to account for the vapor loss, and relative humidity for meteorological  
24 contribution to  $J$ . The parameterization results showed that our models were able to produce plausible predictions  
25 for boreal forest environments, heavily polluted environments, and biogenic environments with high relative  
26 humidity. We further tested the models in the global simulation module Tracer Model 5 (TM5, massive parallel  
27 version) to simulate particle number size distribution across 14 global atmospheric measurement sites. The  
28 simulated results showed satisfactory predictions on particle number concentrations for all the tested environments,  
29 with significant improvement in the nucleation mode, and better prediction accuracy for Aitken and accumulation



30 modes compared to the binary sulfuric acid-organic vapor model in Riccobono (2014). Our study has successfully  
31 provided powerful tools to predict  $J_5$  on a global scale across various environment types using the most essential  
32 and more accessible variables involved in the NPF processes. Essentially, this work reinforces the necessity for  
33 global research into the investigation of environment-oriented meteorology-involved NPF processes.

## 34 **1 Introduction**

35 Atmospheric new particle formation (NPF) is a natural phenomenon observed globally (Bousiotis et al., 2021;  
36 Brean et al., 2023; Gordon et al., 2017; Kerminen et al., 2018; Nieminen et al., 2018). As particles form and grow  
37 on regional scales, they can reach large enough sizes at which they can act as cloud condensation nuclei (CCN) for  
38 water vapor to condense onto when forming clouds. This process affects cloud properties (Roldin et al., 2011;  
39 Sanchez et al., 2016; Spracklen et al., 2008) and ultimately the global climate depending on the particle numbers,  
40 sizes and their chemical compositions (Bellouin et al., 2020; Calvo et al., 2013; Uno et al., 2020). Particle formation  
41 rate ( $J$ ) is an essential parameter describing the NPF intensity, which is often utilized to represent NPF in global  
42 models to simulate the effect of NPF on cloud properties and radiative forcing on Earth. To derive a representative  
43 parametrization of  $J$  for global simulation, we require a broad understanding of NPF in different environments  
44 temporally and spatially. That being the case, the atmospheric measurements of both particle number size  
45 distributions and NPF precursor vapors are essential to obtain for the atmospheric observations and model  
46 developments.

47 The NPF processes have been investigated and parameterized based on particle formation mechanism theories  
48 (Chang et al., 2009; Kulmala et al., 2001; Lehtinen and Kulmala, 2003), field measurements from specific  
49 environments, such as pristine boreal forests (Kulmala et al., 2001; Nieminen et al., 2011; Paasonen et al., 2010),  
50 urban cities (Salma et al., 2011, 2016, 2021; Salma and Németh, 2019; Zhang et al., 2010), rural area (Lee et al.,  
51 2019; Yli-Juuti et al., 2009), marine environment (Zhang et al., 2010), and also chamber experiments (Kirkby et  
52 al., 2011; Lehtipalo et al., 2018). In addition to neutral particle formation mechanisms, the ion-induced nucleation  
53 is also covered in  $J$  parameterizations (e.g. Nieminen et al., 2011; Määttänen et al., 2018). The existing literature  
54 primarily focused on the particle activation and survival of nucleation mode particles down to 1.5 nm, involving  
55 complex micro-physics of aerosol particles, such as nanometer clusters production, losses due to clusters  
56 coagulation and growth (Bousiotis et al., 2021; Chu et al., 2019; Kerminen et al., 2018; Nieminen et al., 2018).  
57 Furthermore, distinct effects on particle formation rates influenced by the same factors were seen under comparable



58 environmental settings. However, these environment-specific models typically have limited application for global  
59 simulation implementations that encompass the diverse atmospheric conditions on Earth.

60 To simulate particle formation rates, one usually starts from the nucleation mode size range. Global modelers have  
61 been facing great challenges in simulating nucleation mode particles because large-scale models have limited  
62 capabilities in treating the complicated aerosol dynamics taking place in the sub-5 nm particle size range. The  
63 formation rate at 5 nm is shown to be important because after sizes of about a few nm in diameter, particle growth  
64 rates show relatively limited variability in different environments (Kulmala et al., 2022a, b, 2023). In addition, we  
65 currently do not have a good enough theoretical understanding on the processes dictating particle growth rates at  
66 the smallest sizes, nor the survival of such particles from coagulation scavenging (e.g. Cai et al., 2022; Tuovinen  
67 et al., 2022; Marten et al., 2022).

68 The essential parameters for  $J$  parameterizations should include at least one type of precursor vapor, some may  
69 also cover meteorological parameters, and the sinks for vapors and particles. For instance, sulfuric acid ( $\text{H}_2\text{SO}_4$ ) as  
70 the most known precursor vapor plays a critical role in particle formation and growth processes due to its low  
71 volatility (Kulmala et al., 2004; Mylly et al., 2019). In the earlier parameterizations of NPF mechanism,  $J$   
72 correlated (linearly or squared) with  $\text{H}_2\text{SO}_4$  concentrations in various environments (Paasonen et al., 2010). In  
73 terms of meteorology, air temperature ( $T$ ), relative humidity (RH), global solar radiation (GRad), wind speed (WS),  
74 and wind direction influence the particle formation rates in certain environments as well (Laarne et al., 2022; Salma  
75 et al., 2021; Zaidan et al., 2018). The variation of  $T$  can influence the precursor vapor formation and stability of  
76 NPF processes: a higher  $T$  can enhance the biogenic emissions that participate in particle formation in a boreal  
77 forest (Dada et al., 2017; Nieminen et al., 2015), while a lower  $T$  favored the  $\text{H}_2\text{SO}_4$ -amine clusters stability in a  
78 megacity (Deng et al., 2020). RH can impact the precursor vapor formations as well as the aerosol formation rates  
79 (Ding et al., 2021; Hellmuth, 2006). The variation of RH is dependent upon  $T$  so that the rise of  $T$  during daytime  
80 increases the planetary boundary layer height (PBLH), which in turn dilutes the air mixture and decreases the RH  
81 (Liu et al., 2018) as well as particle number concentrations (Mazon et al., 2016) in the atmosphere. For condensable  
82 vapor loss, we usually include the term condensation sink (CS), which describes the loss rate of condensable vapors  
83 to aerosol particles, and it typically declines before an NPF event starts.  $\text{H}_2\text{SO}_4$  concentrations, on the other hand,  
84 increase due to the reduction in CS, which means that the condensable vapors are not lost onto the aerosol particles  
85 as efficiently as they would be at greater CS values (Hellmuth, 2006; Kulmala et al., 2012).

86 In general, the developed  $J$  models underestimate the observed particle number concentration, which may be  
87 attributed to NPF schemes being poorly represented in these models. Many  $J$  parameterization works were  
88 conducted focusing on the formation mechanisms from sulfuric acid (Paasonen et al., 2010), sulfuric acid-water



89 (Määttä et al., 2018), sulfuric acid-ammonia (Glasoe et al., 2015), and sulfuric acid-organic vapor (Paasonen et  
90 al., 2010; Riccobono et al., 2014). However, some models are likely applicable only to certain types of environment,  
91 or they primarily cover the microphysics of the particle nucleation at sub-3 nm range, where the nucleated clusters  
92 face higher instability due to the higher evaporation rates than condensation rates (Deng et al., 2021; Wang et al.,  
93 2011). Bergman (2022) attempted an organic-vapor-based NPF scheme in addition to the commonly used binary  
94 water-sulfuric-acid-based scheme to simulate global particle formation and number concentrations. This scheme  
95 improved the simulated number concentrations across the observation stations, although they were still  
96 underestimated compared to the observations, suggesting that the parameterization of early growth of particles to  
97 5 nm diameter still requires improvement.

98 To predict the particle formation rate at 5 nm originating from NPF and subsequent growth, as well as to understand  
99 and predict the climatic impacts caused by NPF and initial growth in global scale, we parameterize particle  
100 formation rates ( $J$ ) at 5 nm using combined measurement data from six different environments: Hyytiälä (boreal  
101 forest close to rural environment, Finland), Beijing (megacity, China), Värriö (remote boreal forest, Finland),  
102 Budapest (urban, Hungary), Agia Marina Xyliatos (rural, Cyprus) and Manacapuru (Amazonian basin, Brazil). The  
103 parameterizations of  $J$  were based on the analysis of atmospheric particle number-size distributions. Sulfuric acid  
104 concentrations, RH and CS are the main input variables in the parameterization models. By including information  
105 from various types of environments, we will be able to demonstrate whether our models can adequately explain the  
106 formation rate of 5 nm particles on a wider environmental scale. The parameterized models are then incorporated  
107 into EC-Earth models to simulate particle formation rates in the global scale (the European community Earth-  
108 System Model, EC-Earth, chemistry transport model TM5: Tracer Model 5, version TM5-chem-v3.0, details in  
109 supplement) (Huijnen et al., 2010).

110 This work aims to provide an effective tool for global particle formation rate estimations. Our parameterizations  
111 have three main features: (1) the number of inputs is limited to be the most essential parameters involved in NPF  
112 process, (2) they do not involve complex microphysics at particles smaller than 5 nm, and (3) they cover a wide  
113 range of environment types. These features will enhance the applicability of the parameterizations for the purpose  
114 of global model application.



## 115 **2 Measurement locations and instrumentation**

116 This study includes measurements from six different sites representing different environmental conditions. A  
117 summary for all locations and the instrumentation used is given in Table S1. Figure 1 shows the map of the  
118 measurement sites included in this study.

### 119 **2.1 Measurement sites**

#### 120 **2.1.1 Rural boreal forest environment: Hyytiälä, Finland**

121 The measurement data were obtained from the SMEAR II-station (Station for Measuring Ecosystem–Atmosphere  
122 Relations), situated in a Scots pine (*Pinus sylvestris*) forest in Hyytiälä (61.1 N, 24.17 E; 181 m (a.s.l.); Hari and  
123 Kulmala, 2005), southern Finland. This measurement site is described as having a rural regional background with  
124 minimal anthropogenic emission. Hyytiälä data covered the period from 21 March 2016 to 18 August 2019.

#### 125 **2.1.2 Remote sub-arctic boreal forest: Värriö, Finland**

126 The SMEAR I measurement station (67°45'31° N, 29°36'41° E, 390 m a.s.l.) was built on the top of Kotovaara hill  
127 located in north-eastern Finland. Similar to Hyytiälä, the site is also a rural background covered mainly by Scots  
128 pine (*Pinus sylvestris*) forest located at the north side of the Värriö fell range. However, it is affected by potential  
129 polluted air mass that comes from Kola peninsula rather than local industrial pollutants. A detailed description of  
130 SMEAR I station can be found in (Kyrö et al., 2014). The data used from Värriö were from 5 April to 13 August  
131 2019.

#### 132 **2.1.3 Polluted megacity: Beijing, China**

133 In Beijing, the measurements were performed at the west campus of the Beijing University of Chemical Technology  
134 (BUCT, 39.94° N, 116.30° E, 20 m a.s.l.). The sampling took place from outside the window on the 5<sup>th</sup> floor of the  
135 university building close to a street with busy traffic. For more details on the description of BUCT measurement  
136 site, see Liu et al., 2020. The data were available from 29 May 2018 to 3 April 2019.



#### 137 **2.1.4 Urban site: Budapest, Hungary**

138 The measurements took place at the Budapest platform for Aerosol Research and Training (BpART) Laboratory  
139 (47.47° N, 19.06° E; 115 m a.s.l.) of the Eötvös Loránd University situated on the bank of the river Danube. The  
140 site represents a mixed average atmosphere of the city center (Salma et al., 2016). The data were obtained from 22  
141 March to 17 April 2018.

#### 142 **2.1.5 Mediterranean rural site: Agia Marina, Cyprus**

143 The measurements were conducted at the Agia Marina Xyliatou (AMX) station (35.03° N, 33.05° E; 532 m a.s.l.)  
144 of the Cyprus Atmospheric Observatory (CAO). The site represents a rural background location situated at the  
145 foothills of Troodos mountains, with agriculture land in the vicinity. The data were obtained between 22 February  
146 and 3 March 2018. For more details about the site, see e.g. Baalbaki et al., (2021).

#### 147 **2.1.6 Amazonian basin: Manacapuru, Brazil**

148 The Manacapuru measurement site was in a pastureland 70 km west of Manaus, Brazil, in central Amazonia. This  
149 site receives air mass from various resources, including rural, biogenic and anthropogenic from the nearby  
150 municipality (Manaus). The trace gases and meteorological measurements were performed during the  
151 GoAmazon2014/5 campaign at the T3 site (3.2133° S, 60.5987° W 50 m a.s.l.), 10 km northeast of Manacapuru,  
152 Brazil (Martin et al., 2016; Schiro et al., 2018). A more detailed description of the measurement site can be found  
153 in (Myers et al., 2022). The data covered the time period from 22 August 2014 to 9 October 2014.

### 154 **2.2 Instrumentation**

#### 155 **2.2.1 Sulfuric acid measurements and proxies**

156 H<sub>2</sub>SO<sub>4</sub> concentrations were measured at all sites, except for the Amazonian basin, using a Chemical Ionization  
157 Atmospheric Pressure interface Time-of-Flight spectrometer (CI-APi-ToF) (Eisele and Tanner, 1993; Jokinen et  
158 al., 2012) with NO<sub>3</sub><sup>-</sup> as the reagent ion and analyzed using tofTools package based on MATLAB software  
159 (Junninen et al., 2010). In the Amazonian basin, H<sub>2</sub>SO<sub>4</sub> concentrations were measured using a selected ion chemical  
160 ionization mass spectrometer (SICIMS), see Myers et al., (2022) for more details. The H<sub>2</sub>SO<sub>4</sub> concentration  
161 measurements were taken from different levels ranging from ground level up to 35 meters above ground level. The  
162 CI-APi-ToFs were calibrated uniformly before the measurement in each location following the technique described



163 by (Kürten et al., 2012), except for the Amazonian basin where the selected ion chemical ionization mass  
164 spectrometer (SICIMS) was calibrated following the scheme described in Mauldin III et al. (1998).  
165 To increase the applicability of our derived parameterization, H<sub>2</sub>SO<sub>4</sub> proxy data from Hyytiälä and Beijing were  
166 included as an additional testing data set. The proxy data were calculated using the proxy specific for the boreal  
167 forest environment and polluted megacity developed by Dada et al., (2020). For Hyytiälä, the sulfuric acid proxy  
168 data ranged from 22 August to 25 December 2016, and 8 March 2018 to 26 February 2019, denoted as Hyytiälä<sub>SAprx</sub>;  
169 For Beijing, the time period was from 15 March to 3 April 2019, denoted as Beijing<sub>SAprx</sub>. The subscript “SAprx”  
170 (SA as in sulfuric acid) in Hyytiälä<sub>SAprx</sub> and Beijing<sub>SAprx</sub> indicates that the datasets utilize H<sub>2</sub>SO<sub>4</sub> concentration from  
171 proxies as input for the testing dataset.

## 172 2.2.2 Particle number size distribution

173 The particle number size distribution (PNSD) measurements were obtained from different types of setups in each  
174 site. Hyytiälä: twin-Differential Mobility Particle Sizers (DMPS; Aalto et al., 2001); Värriö: Differential Mobility  
175 Particle Sizers (DMPS) (Jokinen et al., 2022); Beijing: Particle Size Distribution (PSD) system with a nano-  
176 Differential Mobility Analyzer (DMA) and an Aerodynamic Particle Sizer (APS) (Zhou et al., 2021); Budapest:  
177 flow-switching-type DMPS (6 – 1000 nm; Salma et al., 2016); Cyprus: Neutral cluster and Air Ion Spectrometer  
178 (NAIS) and Scanning Mobility Particle Sizer (SMPS; Baalbaki et al., 2021); Amazonian basin: the measurements  
179 were conducted using SMPS (10 – 1000 nm). It is important to note that we do not aim to compare the PNSD  
180 measurements from all the chosen sites. Instead, the PNSD measurements were used to calculate the formation  
181 rates based on changes in particle number concentrations under local conditions.

## 182 2.2.3 Meteorological variable

183 The meteorological variables included in this study are relative humidity (RH, %) and ambient temperature ( $T$ , °C).  
184 In Hyytiälä, RH and  $T$  were measured at 16.8 m using Rotronic MP102H RH sensor (Rotronic Hygromet MP102H  
185 with Hygroclip HC2–S3, Rotronic AG, Bassersdorf, Switzerland); In Värriö, RH and  $T$  were measured by a  
186 Rotronic MP106A captive sensor; In Beijing, RH and  $T$  were monitored by Vaisala weather station (AWS310); In  
187 Budapest, RH and  $T$  were monitored using Vaisala HMP45D temperature and humidity probe, and Vaisala  
188 WAV15A anemometer located on on-site of the BpART Lab; In Cyprus, RH and  $T$  were measured by a  
189 meteorological station in a nearby village (35.01° N, 33.05° E), 2.85 km away from the measurement site; In  
190 Amazonian basin, RH and  $T$  were measured at the Atmospheric Radiation Measurement (ARM) user facility.



## 191 2.3 Data analysis

### 192 2.3.1 Calculation of particle formation rates

193 To develop more inclusive and generalized models, the parameterization included data from both NPF event days  
194 and non-event days. This approach recognizes that the production of atmospheric secondary particles from non-  
195 NPF events (days with no apparent particle growth) is becoming more significant in a world with growing  
196 anthropogenic influence (Kulmala et al., 2022a). Such a measure would increase the applicability of our models on  
197 a global scale.

198 The observed particle formation rates ( $J_5$ ) at 5 nm were calculated from the measured PNSD according to Equation  
199 1 (Kulmala et al., 2012).

$$200 J_{d_p} = \frac{dN_{d_p}}{dt} + CoagS_{d_p} * N_{d_p} + \frac{GR}{\Delta d_p} * N_{d_p} \quad (\text{Eq. 1})$$

201 The first term  $dN_{d_p}/dt$  is the change in concentration in the size bin, 5–9 nm. The second term  $CoagS_{d_p}$  is the  
202 coagulation sink, which describes the 5-9 nm particle losses due to coagulation with larger particles calculated from  
203 the PNSD at each measurement site (Kulmala et al., 2012). The third term describes the loss of particles due to  
204 their growth out of the size bin. Here, we calculated the growth rates (GR) of 5–9 nm particles using the maximum  
205 concentration method (Kulmala et al., 2012) for days classified as NPF event days as described by Dal Maso et al.,  
206 (2005). The GR for non-event days was approximated using the normalized PNSD from the sum of non-NPF events  
207 at each site. Such approximation is validated for several locations as a ‘quiet NPF’ occurs with the similar GR as  
208 that on NPF event days (Kulmala et al., 2022a).

### 209 2.3.2 Extrapolation of particle formation rates

210 For Budapest and the Manacapuru (Amazonian basin), the particle formation rates were calculated from PNSD  
211 measurements at 6 nm and 10 nm, respectively. Therefore, we obtained  $J_5$  by extrapolating from  $J_6$  and  $J_{10}$   
212 respectively. The  $J_5$  extrapolation followed the analytical formula derived by Kerminen and Kulmala (2002). We  
213 extrapolated  $J_5$  from  $J_6$  for Budapest. For Manacapuru, the extrapolations were done separately for  $J_{10}$  (wet season)  
214 and  $J_{14}$  (dry season), due to the particle size limit of the measurement instrument.





### 215 **2.3.3 Condensation and coagulation sink (CS and CoagS)**

216 The CS and CoagS were calculated from the measured PNSD data for each site using the method proposed by  
217 Kulmala et al., (2012). To ensure the comparability between all locations, both CS and CoagS were calculated  
218 without the correction for hygroscopic growth.

### 219 **2.3.4 Datasets**

220 The parameterizations were developed using the combined dataset from all six measurement sites in hourly time  
221 resolution. Data points were selected considering detection limit of the instruments and therefore, the filters were  
222 set to be  $J_5 > 1 \times 10^{-5} \text{ cm}^{-3} \text{ s}^{-1}$ ,  $\text{H}_2\text{SO}_4$  concentration  $> 5 \times 10^3 \text{ cm}^{-3}$ ,  $\text{RH} \in [0, 100] \%$  and  $\text{CS} > 1 \times 10^{-5} \text{ s}^{-1}$ . The complete  
223 dataset was afterwards randomly resampled into a training set (75% from the complete dataset) and a testing set  
224 (25% the rest of the complete dataset) for parameterization. In model testing, we included two additional inputs  
225 from  $\text{H}_2\text{SO}_4$  concentration proxies developed by Dada et al., (2020) from Hyytiälä and Beijing. The detailed number  
226 of data points per site are shown in Table 1. The data distribution and comparison of each input variable are  
227 displayed in Figure S2, where the overall variations of the input variables across the six sites are distinct in their  
228 range and intensity, which pronounces the inclusivity of model training for a wider application in global  
229 environments.

230

## 231 **3 Parameterization of $J_5$**

### 232 **3.1 Derivation of parameterization models**

233 We derived the parametrized  $J_5$  based on the input variables ( $\text{H}_2\text{SO}_4$ , RH, CS), which were chosen based on field  
234 observations that highlighted their roles in the particle formation mechanism across various environments (Baalbaki  
235 et al., 2021; Dada et al., 2020; Kerminen et al., 2018; Myers et al., 2022; Quéléver et al., 2022; Salma et al., 2016,  
236 2021; Yan et al., 2021). It has been discovered that NPF events occur favorably under lower RH, for example in  
237 boreal forests (Dada et al., 2018; Yao et al., 2018), Mediterranean regions (Debevec et al., 2018), from CLOUD  
238 chamber experiment (Duplissy et al., 2016) and model studies (Hamed et al., 2011). RH was shown to be seasonally  
239 related to cloudiness and global radiation, so that a decreasing global radiation can lead to an increased RH and  
240 cloudiness in the troposphere (Ruosteenoja and Räisänen, 2013). To reduce the model complexity, we opted to use  
241 RH as an indirect indicator of global radiation. A lower CS facilitates the occurrence of NPF events even in



242 contrasting environments with distinct types of condensable vapor. For example, CS can act as a sink for  
243 anthropogenic vapors in a megacity (Wang et al., 2011) and for biogenic vapors in a clean boreal forest (Dada et  
244 al., 2017; Tuovinen et al., 2020).

245 We tested with  $T$  as an input variable during model derivation and training. However, the modelled results did not  
246 show improvement compared to the current parameterization, suggesting that  $T$  provided redundant information  
247 for describing particle formation in the context of our model's global application.

248 As for precursor vapor types other than sulfuric acid, although the highly oxygenated organic molecules (HOMs)  
249 and ammonia ( $\text{NH}_3$ ) have been discovered to play a significant role in particle formation process (Bianchi et al.,  
250 2019; Lehtipalo et al., 2018), we were unable to include these vapor concentrations owing to limited data  
251 availability from the chosen measurement sites. So far, long-term measurements ( $> 1$  year) of HOMs, matching the  
252 time range covered by other variables, are only available in Hyytiälä from a CI-API-ToF mass spectrometer.  
253 However, this is not the case at other sites, limiting our ability to have simultaneous HOMs data across all  
254 environments included in this study. Similarly, the  $\text{NH}_3$  concentrations either did not cover the same time period  
255 as other variables or were unavailable for the other environments.

### 256 3.1.1 Different versions of the parameterization models

257 The derived model functional forms are as follows:

258 Model 1 (the baseline model, Eq. 2) presents the simplest particle formation mechanism based solely on the  
259 abundance of the precursor vapor  $\text{H}_2\text{SO}_4$  concentrations in the atmosphere. The coefficient  $k_1$  serves as a scaling  
260 coefficient that represents the activation rate of clusters in the presence of  $\text{H}_2\text{SO}_4$  molecules during cluster  
261 formation (Kulmala et al., 2006; Paasonen et al., 2010).

$$262 J_5 = k_1 \times [\text{H}_2\text{SO}_4] \quad (\text{Eq. 2})$$

263 Model 2 (Eq. 3) introduces RH in addition to model 1 to partially represent the effect of the changing meteorological  
264 conditions relating to the global radiation and ambient water vapor content on  $J_5$  in general in different types of  
265 environments (Dada et al., 2017; Hamed et al., 2011; Li et al., 2019). The coefficient  $k_2$  serves as a scaling  
266 coefficient and shown as the activation efficiency of the nucleated clusters.

$$267 J_5 = k_2 \times [\text{H}_2\text{SO}_4] \times \text{RH}^{k_{\text{RH}}} \quad (\text{Eq. 3})$$

268 Model 3 (Eq. 4) includes, in addition to model 2, the sink factor CS. The CS factor represents the loss of available  
269 vapors participating in particle formation and growth in the sub-5 nm range to background particles. It can also  
270 indirectly represent the particle survivability till 5 nm, as the loss of vapor concentration from gas phase will hinder



271 the formation and growth of particles/clusters before they reach 5 nm. The coefficient  $k_3$  serves as a scaling  
272 coefficient for the activation and survival efficiency of the nucleated clusters.

$$273 \quad J_5 = k_3 \times [\text{H}_2\text{SO}_4] \times \text{RH}^{k_{\text{RH}}} \times \text{CS}^{k_{\text{CS}}} \quad (\text{Eq. 4})$$

274 Model 4 (Eq. 5), additionally accounts for the formation of  $\text{H}_2\text{SO}_4$  multimers in the gas phase prior to cluster  
275 formation as assumed by the kinetic theory (McMurry and Friedlander, 1979), the coefficient  $k_{\text{SA}}$  represents the  
276 number of  $\text{H}_2\text{SO}_4$  molecules (2, 3, 4, etc...). Therefore,  $k_4$  in this case is not the activation coefficient anymore but  
277 includes both the collision frequency and the probability of a stable particle formation after the collision (Sihto et  
278 al., 2006; Weber et al., 1996).

$$279 \quad J_5 = k_4 \times [\text{H}_2\text{SO}_4]^{k_{\text{SA}}} \times \text{RH}^{k_{\text{RH}}} \times \text{CS}^{k_{\text{CS}}} \quad (\text{Eq. 5})$$

### 280 3.2 Model training results

281 To derive a parametrized  $J_5$  based on precursor and other input variables from the training dataset, we used the  
282 “*fmincon*” optimization algorithm in MATLAB to retrieve the values of each coefficient ( $k_1$ - $k_4$ ,  $k_{\text{SA}}$ ,  $k_{\text{RH}}$  and  $k_{\text{CS}}$ )  
283 from the training dataset. The coefficients obtained for each of the models can be found in Table 2. The derived  
284 models with the optimized coefficients were applied to the testing datasets and compared with the observed  $J_5$  and  
285 the parametrized  $J_5$ . We evaluated the performance of each model based on the data distribution, the resulting  
286 deviation from observation and its uncertainty. To maintain the global model’s simplicity, the parameterization  
287 covered both daytime and night-time data for all sites in all models.

288 Figure S3 presents the measured to modelled  $J_5$  from model 1-4 using training dataset from six measurement sites,  
289 including the slopes and coefficient of determination ( $R^2$ ). Overall, by comparing model 1 (Fig. S3a) and model 2  
290 (Fig. S3b), we observed an improvement in the model performance with the inclusion of RH. The  $R^2$  value  
291 improved from 0.28 to 0.44, and the slope increased from 0.29 to 0.56. This observation confirmed the importance  
292 of considering meteorological impact when parameterizing  $J_5$ . By further including CS in model 3, the model  
293 improved further (Fig. S3c), with the  $R^2$  increasing from 0.44 to 0.49, and the slope from 0.56 to 0.62. To further  
294 introduce the kinetic theory and the formation of  $\text{H}_2\text{SO}_4$  dimers and other multimers, we added an exponent over  
295  $\text{H}_2\text{SO}_4$  in model 4 (Fig. S3d). This addition showed a further improved correlation and slope between the measured  
296 or modeled data for the training datasets ( $R^2 = 0.57$ , slope = 0.76). In subsequent testing, model 4 generally  
297 outperformed the other models (see section 4, Fig. 2).



### 298 3.3 Model evaluations

#### 299 3.1.1 MAE and RMSE

300 We computed the mean absolute errors (MAE), root mean square errors (RMSE) for each model using the testing  
301 dataset to gain a better understanding of the models' performance. The numerical values of MAE and RMSE are  
302 given in Table S3.

303 The MAE calculation equation is as follows:

$$304 \quad MAE = \frac{1}{n} \sum_{i=1}^n |y_i - \hat{y}_i| \quad (\text{Eq. 6})$$

305 where  $n$  is the number of data points (here it is the total number of data points from testing set, see Table 1),  $y_i$  is  
306 the observed value, and  $\hat{y}_i$  denotes the predicted value. MAE measures the accuracy of models' prediction power,  
307 by quantifying the average magnitude of errors between observed and predicted values (Chai and Draxler, 2014).

308 A lower model error is manifested by a lower MAE value.

309 The RMSE is calculated as the square root of the difference between the measured ( $y_i$ ) and predicted ( $\hat{y}_i$ )  $J_5$  values  
310 normalized by the number of data points.

$$311 \quad RMSE = \sqrt{\frac{1}{n} \sum_{i=1}^n (y_i - \hat{y}_i)^2} \quad (\text{Eq. 7})$$

312 RMSE also measures the average magnitude of errors of models. However unlike MAE, RMSE squares the errors  
313 giving greater weight to larger errors and penalizing them more heavily (Chai and Draxler, 2014). Therefore, RMSE  
314 values reveal whether the models' performances are highly influenced by large prediction errors. Similar to MAE,  
315 lower RMSE values indicate better model performance.

316 Figure S4 (upper panel) depicts a declining trend of the overall MAE from models 1 to 4 (Eqs. 2-5). For the  
317 environmental types investigated in this study, the MAE values of the four models from all sites are lower than 1,  
318 indicating that the mean differences on the magnitude for  $J_5$  are minor when utilizing the parameter settings from  
319 our models. However, Budapest stands out due to the apparent higher MAE, potentially highlighting the distinct  
320 NPF mechanism in Budapest compared to the other sites as well as the seasonal limitations on its data (spring 2018  
321 only).



322 The RMSE values increased as more parameters were added into the model, peaking for model 3 (Fig. S4, lower  
323 panel), even though model 3 can predict  $J_5$  for multiple types of environments on a satisfactory level. We can see  
324 that from model 1 to model 2, the inclusion of RH increased the model errors more compared to the addition of CS  
325 from model 2 to model 3. However, the RMSE values dropped significantly when  $H_2SO_4$  was allowed to vary with  
326 an exponent  $k_{SA}$  in model 4 in the presence of both RH and CS.

327 Based on the results summarized above, models 3 and 4 (Eqs. 4&5) seem to be the most promising for global  $J_5$   
328 prediction among all model types owing to their low MAE values. However, the lower RMSE for model 4 showed  
329 its outperformance to model 3.

### 330 3.1.2 Akaike Information Criterion

331 The Akaike Information Criterion (AIC) is a statistical measure that helps to evaluate the goodness-of-fit of a  
332 statistical model. We use AIC as an evaluation tool because it can evaluate models with different number of  
333 parameters and complexities, ensuring a balanced assessment. Eventually, it allows us to select the model with the  
334 best balance between the model complexity and goodness-of-fit. The parameters used to calculate the AIC for each  
335 site are shown in Tables S4-S6. A lower AIC score indicates a superior goodness-of-fit and a lower tendency for  
336 model overfitting. The relative likelihood term ( $L$ ,  $L = e^{(AIC_{min}-AIC_i)/2}$ ), calculated from AIC scores, reflects the  
337 likelihood that the  $i$ th model minimizes information loss as compared to the model with the lowest AIC. A relative  
338 likelihood of 1 suggests that the model outstands other models in minimizing information loss. For boreal forest  
339 environments (Table. S4), and urban environments (Table. S5), both models 1 and 4 minimized information loss  
340 the most. For rural regions, model 4 (Eq. 5) performs the best (Table. S6). Compared to the baseline model (model  
341 1, Eq. 2), we find that  $H_2SO_4$  is a more powerful parameter than RH or CS in all environments. However, in  
342 Manacapuru, including RH and CS shows clearly an improved predictive accuracy in model 4 (Eq. 5).

## 343 4 Results and discussion

### 344 4.1 Parameterization testing results

345 The scatterplots (Fig. 2) demonstrate the overall performance of the parameterizations from the 4 models (Eqs. 2-  
346 5) using the testing dataset. The overall and site-specific Pearson's coefficients, slopes from robust linear fit  
347 between the measured and modelled  $J_5$ , as well as the number of data points from the testing dataset, can be found  
348 in Table 3. Overall,  $r$  increased significantly for model 2 and 3 (Fig. 2b & 2c,  $r = 0.69$ ,  $r = 0.71$ ) compared to model



349 1 (Fig. 2a,  $r = 0.55$ ) as we include the impacts from meteorology and vapor loss. Model 4 provides the best linear  
350 fit results, implying that the model can predict an overall reliable estimation on  $J_5$  despite the environment types  
351 (Fig. 2d,  $r = 78$ ).

#### 352 **4.1.1 Boreal forests: Hyttiälä and Värriö**

353 Given the boreal forest background, Hyttiälä and Värriö exhibited comparable variations in the distribution of  
354 modelled  $J_5$  values from the four model types. As shown in Figure 3, model 3 ((a3), (b3), (c3)) and model 4 ((a4),  
355 (b4), (c4)) illustrated a more centered data distribution between the modelled and measured  $J_5$ , which confirmed  
356 the strong relationship of the low RH favoring NPF occurrence for the boreal forest environmental conditions (Dada  
357 et al., 2018; Hamed et al., 2011). Notice that the mean  $\text{H}_2\text{SO}_4$  concentration in Värriö is about twice as high as that  
358 in Hyttiälä, opposite to CS which is clearly lower in Värriö (Table S2). The low CS in Värriö compared with  
359 Hyttiälä is primarily due to the lower emission rate of the regional precursor vapors (e.g. Tunved et al., 2006),  
360 leading to the lower observed NPF event frequencies (Kyrö et al., 2014; Neeffjes et al., 2022). We must note that  
361 the Hyttiälä data spanned three years, containing more data points for model training, whereas the Värriö data only  
362 covered the period from April to August 2019, excluding the entire cold season when  $\text{H}_2\text{SO}_4$  concentrations are  
363 significantly lower than those during the warm season (Jokinen et al., 2022). As a result, our model 3 (Fig. 3(a3),  
364 (b3), (c3)) and 4 (Fig. 3(a4), (b4), (c4)) can predict  $J_5$  for boreal forest environment on a satisfactory level, including  
365 the possibility to use the estimated  $\text{H}_2\text{SO}_4$  concentration from proxies as input. Nevertheless, limitations regarding  
366 precursor vapor production rate could potentially influence the prediction accuracy.

#### 367 **4.1.2 Urban-influenced: Beijing and Budapest**

368 In anthropogenic emissions dominated region, such as Beijing, the measured and modelled  $J_5$  are well aligned  
369 around the 1:1 line using model 3 (Fig. 3(d3), (e3), (f3)), and model 4 (Fig. 3 (d4), (e4), (f4)). In Beijing, a polluted  
370 megacity, the dominating precursor type has been found to be  $\text{H}_2\text{SO}_4$ -amine clusters (Cai et al., 2021). As expected,  
371 the testing result showed dramatic underestimations for Beijing using model 1 with only  $\text{H}_2\text{SO}_4$  concentrations  
372 considered (Fig. 3(d1)), whereas model 3 (Fig. 3(d3)) provided clearly better  $J_5$  predictions, which emphasized the  
373 significance of the meteorology and vapor loss impacts in Beijing. However, the effect of CS in model 3 (Fig.  
374 3(d3)) is small compared to model 2 (Fig. 3(d2)) due to the substantial background aerosol concentrations that  
375 sustain NPF regardless of vapor sinks in such polluted environment. This study did not include amine-related



376 compounds in the formulas because the lack of measured  $\text{NH}_3$  data makes the parallel comparisons difficult among  
377 the chosen sites for model training.

378 For Budapest, a large European city, the underestimates in modelled  $J_5$  are not as much improved as they were for  
379 Beijing when including RH or CS in the parameterization, which is indicative of distinct particle formation  
380 pathways between Beijing and Budapest, even though both sites represent urban background environments. On  
381 one hand, it is worth noting that including RH (model 2, Eq. 3) resulted in a decrease in the correlation coefficients  
382 between the measured and modelled  $J_5$  in Budapest from 0.54 to 0.46 (Table 3). This suggests that the role of RH  
383 in the NPF process in Budapest is less significant than other chosen inputs, despite previous indications that high  
384 RH levels have a strong potential to suppress NPF during non-event days in Budapest (Salma et al., 2021), even  
385 though the RH values in Budapest were considerably higher than those in Beijing (Table S2). On the other hand,  
386 including CS (model 3, Eq. 4) in addition to RH (model 2, Eq. 3) leads to an increase in the correlation coefficients  
387 between the measured and modelled  $J_5$  from 0.46 to 0.61 (Table 3). We used both NPF and non-NPF days during  
388 model training even though it was found that CS was 50% lower during non-NPF events in Budapest than the  
389 values during NPF events (Salma et al., 2016). As a result, it is difficult to determine if the model's performance  
390 gain was entirely brought on by the addition of CS. Otherwise, the results are all in line with the earlier indirect  
391 evidence that chemical species other than  $\text{H}_2\text{SO}_4$  influence the particle growth and possibly NPF process in  
392 Budapest (Salma and Németh, 2019).

393 Based on the testing results, model 3 is more likely to predict a more accurate  $J_5$  for Beijing based on the highest  
394 AIC ratio (except for 1), while model 1 predicts better for Budapest. Notice the fact that  $J_5$  showed distinct levels  
395 of measured  $J_5$  dependence with RH and CS in Beijing and Budapest ( $J_5$  and RH: Beijing:  $r = -0.21$ , Budapest:  $r$   
396  $= -0.1$ ;  $J_5$  and CS: Beijing:  $r = -0.02$ , Budapest:  $r = 0.57$ , Fig. S1).

#### 397 **4.1.3 Mediterranean rural site: Agia Marina, Cyprus**

398 For Cyprus, it appears that meteorology and condensation sink terms have only minor effects on the formation of  
399 5 nm particles in such rural environment under the influence of marine vapors when comparing the results from  
400 testing dataset across models (Fig. 3g). However, including RH improves slightly the correlation between the  
401 modelled and measured  $J_5$  as seen in model 2 ( $r$  rises from 0.42 to 0.49, Table 3). The reduced values of  $r$  in model  
402 3 (Eq. 4) indicate a somewhat reversed impact of CS on  $J_5$ , which requires additional examination as  $J_5$  and CS are  
403 weakly correlated ( $r = 0.03$ , Fig. S1). The  $\text{H}_2\text{SO}_4$  concentration showed a low contribution to  $J_5$  with the exponent  
404 being less than 1 in model 4 (Table 3), which led to a more underestimated modelled  $J_5$  comparing to model 1 (Fig.



405 3(g1), (g4)). This could be an indication that potentially other anthropogenic, biogenic or marine compounds are  
406 of greater contribution to the particle formation processes in Cyprus than H<sub>2</sub>SO<sub>4</sub> (Debevec et al., 2018). Owing to  
407 the orographic conditions, the air mass types approaching to the Cyprus measurement site are mixed, including the  
408 ones from North Africa, Marine, Europe, and northwest/southwest Asia. We should note that the measurements in  
409 Cyprus covered only two weeks in springtime, which limited our quantitative observations in model training for  
410 other seasons compared to sites with long-term measurements. Based on the findings above, model 1 seems to be  
411 the most suitable functional form for the prediction of  $J_5$  in Cyprus.

#### 412 **4.1.4 Amazonian basin: Manacapuru, Brazil**

413 The measured and modelled values of  $J_5$  from the Manacapuru site scatter around the 1:1 line in all the models  
414 (Fig. 3). Previous studies reported high RH levels year-round in the measurement site near Manacapuru (Myers et  
415 al., 2022; Zhao et al., 2022), which is expected to suppress NPF frequency and to lead to lower formation rates.  
416 We observed such suppression effect when taking RH into account as shown by the increased correlation  
417 coefficients from 0.004 to 0.19 (Table 3). Studies from Manacapuru suggested that the epoxide vapors could be a  
418 potential precursor vapor in particle formation because of anthropogenic influences (Paulot et al., 2009), while Xu  
419 et al., (2014) suggested the presence of epoxide vapors can enhance particle nucleation when RH levels increase.  
420 We did not observe apparent improved model performance in model 3 when CS is included, as  $r$  remained almost  
421 unchanged compared to model 2 (Table 3). One factor to consider is that we did not apply hygroscopic growth  
422 factor when calculating CS for Manacapuru to maintain the consistency of the training dataset. However, the impact  
423 of RH on CS, particularly on the actual particle surface area available for H<sub>2</sub>SO<sub>4</sub> uptake, seems to be significant for  
424 high RH environments like Manacapuru (Myers et al. 2022). Another assumption could be that even with the high  
425 CS, it is still low enough to allow sufficient precursor vapors contributing to NPF processes.  
426 These current findings provide evidence for H<sub>2</sub>SO<sub>4</sub> being an effective enough precursor for the particle formation  
427 at 5 nm, as well as the RH stabilization effect on H<sub>2</sub>SO<sub>4</sub> in the atmosphere of Manacapuru. So far, model 4 with a  
428 focus on the H<sub>2</sub>SO<sub>4</sub> concentrations along with meteorology and vapor loss impacts manages to predict  $J_5$  for  
429 biogenic vapor dominated environment like Manacapuru.

#### 430 **5 Tracer model 5 simulation**

431 We simulated the particle number size distribution (PNSD) in EC-Earth global chemical transport model TM5-MP  
432 (Tracer Model 5, Massively Parallel version, details in supplement) by applying it with our  $J_5$  model 1 and 4.





433 Together, we compared our simulation results with the acid-organic binary homogeneous nucleation model from  
434 Riccobono et al. (2014):

$$435 J_{\text{Riccobono}} = k_m \times [\text{H}_2\text{SO}_4]^p \times [\text{BioOxOrg}]^q, \quad (\text{Eq. 8})$$

436 where  $k_m = 3.27 \times 10^{-21} \text{ cm}^6 \text{ s}^{-1}$ ,  $p = 2$  and  $q = 1$ .

437 The details of the 14 tested measurement stations are shown in Table S7. Note that the data from these 14 stations  
438 are independent from any training or testing datasets used in the previous sections of this paper. Here, we essentially  
439 compared the simulated and measured PNSD in three particle modes (nucleation, Aitken, accumulation) from the  
440 entire year 2018 to assess the simulation accuracy among global environments.

441 Figure 4 shows the comparisons of PNSD between the on-site measurements and the TM5-MP simulations. For  
442 biogenic environments, simulations using model 4 shows the closest particle number size distribution to the  
443 measured ones particularly in Aitken mode particles, promoting the sulfuric acid-based nucleation mechanism  
444 involving the source-sink-meteorology even for environment dominated by biogenic vapors. For the Arctic region,  
445 model 4 simulated particle concentrations are overall overestimated, while model 1 simulation shows better  
446 alignment of particle number concentrations around the Aitken mode. This might indicate that the nucleation  
447 process has a lower dependence on the variations of meteorology than we expected. For coastal environments, even  
448 though Utö (Baltic Sea Island) and La Réunion (southern hemisphere island) are located at different hemispheres  
449 and also have different geographical settings, the nucleation mechanisms from models 1 and 4 both show similar  
450 predictions on particle concentrations across particle modes, with larger underestimation in the accumulation mode  
451 for model 1. This once again validates the source-sink-meteorology mechanism in model 4. By observing the ratio  
452 between the simulated and measured particle number concentrations, we can quickly see that the sulfuric acid-  
453 based particle formation mechanisms with (model 4) or without (model 1) meteorology inputs have successfully  
454 narrowed the gap between the simulations and observations across all particle modes, with significant  
455 improvements for the nucleation mode (Fig. 5). The “Total” contains the simulated/measured particle number  
456 concentrations ratio from all particle modes, and it is obviously seen that applying model 4 improves the overall  
457 global PNSD simulation compared with the sulfuric acid-organic vapor binary model from Riccobono et al. (2014).  
458 This observation shows that including the RH and CS is needed for better understanding of the global particle  
459 number size distributions.



## 460 **6 Conclusion**

461 The particle formation rate is one of the key characteristics in new particle formation studies. By utilizing distinct  
462 field measurement data, we can model the particle formation rate and estimate the overall atmospheric aerosol  
463 budget over different environments. We parameterized  $J_5$  in four functional forms using the combined datasets  
464 from six environments, covering boreal forests (Hyytiälä, Värriö), urban sites (a megacity of Beijing and a large  
465 European city of Budapest) and rural environment (Cyprus, Manacapuru). The particle formation schemes involve  
466 the main precursor vapor  $\text{H}_2\text{SO}_4$ , meteorological impacts from RH and the vapor loss from CS. Overall, our models  
467 showed improved performances as RH and CS were taken into consideration. The model evaluations may suggest  
468 that particle formation mechanism is more sensitive to certain factors in specific environments. Sulfuric acid is an  
469 effective precursor vapor in NPF processes for most of the measurement sites we selected for model training.  
470 Nevertheless, relying solely on  $\text{H}_2\text{SO}_4$  generally resulted in a weaker model performance for environments where  
471 the NPF schemes are dominated by biogenic emissions. This suggests that for developing globally applicable  
472 particle formation rate models, more precursor vapor types need to be included alongside  $\text{H}_2\text{SO}_4$ .

473 The purpose of the paper is twofold: first, to address the lack of knowledge regarding global particle formation  
474 rates for particles at 5 nm and larger, and second, to provide a globally applicable semi-empirical parameterization  
475 for the sulfuric acid-based neutral particle formation. The simplicity of the parameterization is demonstrated by  
476 three factors. First, NPF is a widespread occurrence in various types of environments, where the characteristics of  
477 particle formation share common mechanisms involving major precursor types and environmental factors. Second,  
478 the main input  $\text{H}_2\text{SO}_4$  concentrations data can be obtained from field measurements or proxies, from which the  
479 contribution of  $\text{H}_2\text{SO}_4$  to NPF can be directly compared among global sites. Third, we skip the microphysics  
480 complexity of sub-5 nm particles, where the physical and chemical properties differ significantly from those t above  
481 5 nm when discussing particle formation and growth.

482 The limited data availability from certain sites (less than 1 year), such as Budapest, Cyprus and Manacapuru, should  
483 be noted when applying our models. Conclusions drawn from these sites can be more confidently applied to the  
484 specific seasons covered in the model training, such as springs being more representable for Budapest and Cyprus,  
485 and summer to early autumn for Manacapuru.

486 Overall, our parameterization findings show that our models, when including the effects of meteorology and vapor  
487 loss, can predict  $J_5$  on a satisfactory level for various environment types at once. Among the tested models, models  
488 3 and 4 (Eqs. 4 and 5) can be utilized for predicting  $J_5$  in a global scale if (1) the  $\text{H}_2\text{SO}_4$  concentrations are known



489 whether through field measurement or proxies, (2) the meteorology parameter RH is monitored continuously, and  
490 (3) the particle number size distributions are sufficient and assessed to yield CS.

491

492 *Author contributions.* Measurements: NS, RB, CY, LQ, TJ, IS, MV, TW. Data Analysis: XL, LD, MZ, NS, RB,  
493 CY, LQ, IS, PZ. Results interpretation: XL, LD, TN. Discussions: all co-authors. Writing: XL, LD, V-MK, TN.  
494 Comments and revisions: all co-authors.

495 *Data availability.* The data will be available in an open access platform upon publication. The data for the 14 global  
496 measurement sites are from EBAS database (<https://ebas-data.nilu.no/>, last access 13.12.2024).

497 *Conflict of interests.* At least one of the (co-)authors is a member of the editorial board of Aerosol Research.

498 *Code availability.* The MATLAB code used for the parameterization training in this paper will be available in an  
499 open access platform e.g. Zenodo upon final publication.

500

501 *Acknowledgements.* This work was supported by the European Research Council, H2020 European Research  
502 Council (GASPARCON (grant no. 714621), by the EMME-CARE project, which received funding from the  
503 European Union's Horizon 2020 Research and Innovation Programme, under Grant Agreement No. 856612, by the  
504 Hungarian Research, Development and Innovation Office (contract: Advanced 150835), and the Cyprus  
505 Government and by the Research Council of Finland with grant numbers 355330 and by ACCC Flagship funded  
506 by the Academy of Finland grant number 337549. L.D. received funding from the Swiss National Science  
507 Foundation (Ambizione grant number 216181). We are grateful to all the people who have contributed to the  
508 ambient measurements at measurement stations. The Finnish and Cypriot stations are part of the European research  
509 infrastructure ACTRIS. We acknowledge ACTRIS CiGas – Centre for Reactive Trace Gases In Situ Measurements  
510 and CAIS-ECAC – Centre for Aerosol In Situ Measurements for providing operational support to the aerosol and  
511 reactive trace gas instruments at the stations. We also thank Dr. James N. Smith for providing the GoAmazon2014/5  
512 data for Manacapuru.

513



## 514 References

- 515 Aalto, P., Hämeri, K., Becker, E., Weber, R., Salm, J., Mäkelä, J. M., Hoell, C., O’ Dowd, C. D., Hansson, H.-C.,  
516 Väkevä, M., Koponen, I. K., Buzorius, G., and Kulmala, M.: Physical characterization of aerosol particles  
517 during nucleation events, *Tellus B Chem. Phys. Meteorol.*, 53, 344–358,  
518 <https://doi.org/10.3402/tellusb.v53i4.17127>, 2001.
- 519 Baalbaki, R., Pikridas, M., Jokinen, T., Laurila, T., Dada, L., Bezantakos, S., Ahonen, L., Neitola, K., Maisser, A.,  
520 Bimenyimana, E., Christodoulou, A., Unga, F., Savvides, C., Lehtipalo, K., Kangasluoma, J., Biskos, G.,  
521 Petäjä, T., Kerminen, V.-M., Sciare, J., and Kulmala, M.: Towards understanding the characteristics of  
522 new particle formation in the Eastern Mediterranean, *Atmospheric Chem. Phys.*, 21, 9223–9251,  
523 <https://doi.org/10.5194/acp-21-9223-2021>, 2021.
- 524 Bellouin, N., Quaas, J., Gryspeerdt, E., Kinne, S., Stier, P., Watson-Parris, D., Boucher, O., Carslaw, K. S.,  
525 Christensen, M., Daniau, A.-L., Dufresne, J.-L., Feingold, G., Fiedler, S., Forster, P., Gettelman, A.,  
526 Haywood, J. M., Lohmann, U., Malavelle, F., Mauritsen, T., McCoy, D. T., Myhre, G., Mülmenstädt, J.,  
527 Neubauer, D., Possner, A., Rugenstein, M., Sato, Y., Schulz, M., Schwartz, S. E., Sourdeval, O., Storelvmo,  
528 T., Toll, V., Winker, D., and Stevens, B.: Bounding Global Aerosol Radiative Forcing of Climate Change,  
529 *Rev. Geophys.*, 58, e2019RG000660, <https://doi.org/10.1029/2019RG000660>, 2020.
- 530 Bergman, T., Makkonen, R., Schrödner, R., Swietlicki, E., Phillips, V. T. J., Le Sager, P., and van Noije, T.:  
531 Description and evaluation of a secondary organic aerosol and new particle formation scheme within TM5-  
532 MP v1.2, *Geosci. Model Dev.*, 15, 683–713, <https://doi.org/10.5194/gmd-15-683-2022>, 2022.
- 533 Bianchi, F., Kurtén, T., Riva, M., Mohr, C., Rissanen, M. P., Roldin, P., Berndt, T., Crouse, J. D., Wennberg, P.  
534 O., Mentel, T. F., Wildt, J., Junninen, H., Jokinen, T., Kulmala, M., Worsnop, D. R., Thornton, J. A.,  
535 Donahue, N., Kjaergaard, H. G., and Ehn, M.: Highly Oxygenated Organic Molecules (HOM) from Gas-  
536 Phase Autoxidation Involving Peroxy Radicals: A Key Contributor to Atmospheric Aerosol, *Chem. Rev.*,  
537 119, 3472–3509, <https://doi.org/10.1021/acs.chemrev.8b00395>, 2019.
- 538 Bousiotis, D., Pope, F. D., Beddows, D. C. S., Dall’Osto, M., Massling, A., Nøjgaard, J. K., Nordstrøm, C., Niemi,  
539 J. V., Portin, H., Petäjä, T., Perez, N., Alastuey, A., Querol, X., Kouvarakis, G., Mihalopoulos, N., Vratolis,  
540 S., Eleftheriadis, K., Wiedensohler, A., Weinhold, K., Merkel, M., Tuch, T., and Harrison, R. M.: A  
541 phenomenology of new particle formation (NPF) at 13 European sites, *Atmospheric Chem. Phys.*, 21,  
542 11905–11925, <https://doi.org/10.5194/acp-21-11905-2021>, 2021.



- 543 Brean, J., Beddows, D. C. S., Harrison, R. M., Song, C., Tunved, P., Ström, J., Krejci, R., Freud, E., Massling, A.,  
544 Skov, H., Asmi, E., Lupi, A., and Dall’Osto, M.: Collective geographical ecoregions and precursor sources  
545 driving Arctic new particle formation, *Atmospheric Chem. Phys.*, 23, 2183–2198,  
546 <https://doi.org/10.5194/acp-23-2183-2023>, 2023.
- 547 Cai, R., Yan, C., Yang, D., Yin, R., Lu, Y., Deng, C., Fu, Y., Ruan, J., Li, X., Kontkanen, J., Zhang, Q.,  
548 Kangasluoma, J., Ma, Y., Hao, J., Worsnop, D. R., Bianchi, F., Paasonen, P., Kerminen, V.-M., Liu, Y.,  
549 Wang, L., Zheng, J., Kulmala, M., and Jiang, J.: Sulfuric acid–amine nucleation in urban Beijing,  
550 *Atmospheric Chem. Phys.*, 21, 2457–2468, <https://doi.org/10.5194/acp-21-2457-2021>, 2021.
- 551 Cai, R., Deng, C., Stolzenburg, D., Li, C., Guo, J., Kerminen, V.-M., Jiang, J., Kulmala, M., and Kangasluoma, J.:  
552 Survival probability of new atmospheric particles: closure between theory and measurements from 1.4 to  
553 100 nm, *Atmospheric Chem. Phys.*, 22, 14571–14587, <https://doi.org/10.5194/acp-22-14571-2022>, 2022.
- 554 Calvo, A. I., Alves, C., Castro, A., Pont, V., Vicente, A. M., and Fraile, R.: Research on aerosol sources and  
555 chemical composition: Past, current and emerging issues, *Atmospheric Res.*, 120–121, 1–28,  
556 <https://doi.org/10.1016/j.atmosres.2012.09.021>, 2013.
- 557 Chai, T. and Draxler, R. R.: Root mean square error (RMSE) or mean absolute error (MAE)? – Arguments against  
558 avoiding RMSE in the literature, *Geosci. Model Dev.*, 7, 1247–1250, [https://doi.org/10.5194/gmd-7-1247-](https://doi.org/10.5194/gmd-7-1247-2014)  
559 2014, 2014.
- 560 Chang, L.-S., Schwartz, S. E., McGraw, R., and Lewis, E. R.: Sensitivity of aerosol properties to new particle  
561 formation mechanism and to primary emissions in a continental-scale chemical transport model, *J.*  
562 *Geophys. Res. Atmospheres*, 114, <https://doi.org/10.1029/2008JD011019>, 2009.
- 563 Chu, B., Kerminen, V.-M., Bianchi, F., Yan, C., Petäjä, T., and Kulmala, M.: Atmospheric new particle formation  
564 in China, *Atmospheric Chem. Phys.*, 19, 115–138, <https://doi.org/10.5194/acp-19-115-2019>, 2019.
- 565 Dada, L., Paasonen, P., Nieminen, T., Buenrostro Mazon, S., Kontkanen, J., Peräkylä, O., Lehtipalo, K., Hussein,  
566 T., Petäjä, T., Kerminen, V.-M., Bäck, J., and Kulmala, M.: Long-term analysis of clear-sky new particle  
567 formation events and nonevents in Hyytiälä, *Atmospheric Chem. Phys.*, 17, 6227–6241,  
568 <https://doi.org/10.5194/acp-17-6227-2017>, 2017.
- 569 Dada, L., Chellapermal, R., Buenrostro Mazon, S., Paasonen, P., Lampilahti, J., Manninen, H. E., Junninen, H.,  
570 Petäjä, T., Kerminen, V.-M., and Kulmala, M.: Refined classification and characterization of atmospheric  
571 new-particle formation events using air ions, *Atmospheric Chem. Phys.*, 18, 17883–17893,  
572 <https://doi.org/10.5194/acp-18-17883-2018>, 2018.



- 573 Dada, L., Ylivinkka, I., Baalbaki, R., Li, C., Guo, Y., Yan, C., Yao, L., Sarnela, N., Jokinen, T., Daellenbach, K.  
574 R., Yin, R., Deng, C., Chu, B., Nieminen, T., Wang, Y., Lin, Z., Thakur, R. C., Kontkanen, J., Stolzenburg,  
575 D., Sipilä, M., Hussein, T., Paasonen, P., Bianchi, F., Salma, I., Weidinger, T., Pikridas, M., Sciare, J.,  
576 Jiang, J., Liu, Y., Petäjä, T., Kerminen, V.-M., and Kulmala, M.: Sources and sinks driving sulfuric acid  
577 concentrations in contrasting environments: implications on proxy calculations, *Atmospheric Chem. Phys.*,  
578 20, 11747–11766, <https://doi.org/10.5194/acp-20-11747-2020>, 2020.
- 579 Debevec, C., Sauvage, S., Gros, V., Sellegri, K., Sciare, J., Pikridas, M., Stavroulas, I., Leonardis, T., Gaudion, V.,  
580 Depelchin, L., Fronval, I., Sarda-Esteve, R., Baisnée, D., Bonsang, B., Savvides, C., Vrekoussis, M., and  
581 Locoge, N.: Driving parameters of biogenic volatile organic compounds and consequences on new particle  
582 formation observed at an eastern Mediterranean background site, *Atmospheric Chem. Phys.*, 18, 14297–  
583 14325, <https://doi.org/10.5194/acp-18-14297-2018>, 2018.
- 584 Deng, C., Fu, Y., Dada, L., Yan, C., Cai, R., Yang, D., Zhou, Y., Yin, R., Lu, Y., Li, X., Qiao, X., Fan, X., Nie,  
585 W., Kontkanen, J., Kangasluoma, J., Chu, B., Ding, A., Kerminen, V.-M., Paasonen, P., Worsnop, D. R.,  
586 Bianchi, F., Liu, Y., Zheng, J., Wang, L., Kulmala, M., and Jiang, J.: Seasonal Characteristics of New  
587 Particle Formation and Growth in Urban Beijing, *Environ. Sci. Technol.*, 54, 8547–8557,  
588 <https://doi.org/10.1021/acs.est.0c00808>, 2020.
- 589 Deng, C., Cai, R., Yan, C., Zheng, J., and Jiang, J.: Formation and growth of sub-3 nm particles in megacities:  
590 impact of background aerosols, *Faraday Discuss.*, 226, 348–363, <https://doi.org/10.1039/D0FD00083C>,  
591 2021.
- 592 Ding, J., Dai, Q., Zhang, Y., Xu, J., Huangfu, Y., and Feng, Y.: Air humidity affects secondary aerosol formation  
593 in different pathways, *Sci. Total Environ.*, 759, 143540, <https://doi.org/10.1016/j.scitotenv.2020.143540>,  
594 2021.
- 595 Duplissy, J., Merikanto, J., Franchin, A., Tsagkogeorgas, G., Kangasluoma, J., Wimmer, D., Vuollekoski, H.,  
596 Schobesberger, S., Lehtipalo, K., Flagan, R. C., Brus, D., Donahue, N. M., Vehkamäki, H., Almeida, J.,  
597 Amorim, A., Barmet, P., Bianchi, F., Breitenlechner, M., Dunne, E. M., Guida, R., Henschel, H., Junninen,  
598 H., Kirkby, J., Kürten, A., Kupc, A., Määttänen, A., Makhmutov, V., Mathot, S., Nieminen, T., Onnela,  
599 A., Praplan, A. P., Riccobono, F., Rondo, L., Steiner, G., Tome, A., Walther, H., Baltensperger, U.,  
600 Carslaw, K. S., Dommen, J., Hansel, A., Petäjä, T., Sipilä, M., Stratmann, F., Vrtala, A., Wagner, P. E.,  
601 Worsnop, D. R., Curtius, J., and Kulmala, M.: Effect of ions on sulfuric acid-water binary particle  
602 formation: 2. Experimental data and comparison with QC-normalized classical nucleation theory, *J.*  
603 *Geophys. Res. Atmospheres*, 121, 1752–1775, <https://doi.org/10.1002/2015JD023539>, 2016.



- 604 Eisele, F. L. and Tanner, D. J.: Measurement of the gas phase concentration of H<sub>2</sub>SO<sub>4</sub> and methane sulfonic acid  
605 and estimates of H<sub>2</sub>SO<sub>4</sub> production and loss in the atmosphere, *J. Geophys. Res. Atmospheres*, 98, 9001–  
606 9010, <https://doi.org/10.1029/93JD00031>, 1993.
- 607 Glasoe, W. A., Volz, K., Panta, B., Freshour, N., Bachman, R., Hanson, D. R., McMurry, P. H., and Jen, C.: Sulfuric  
608 acid nucleation: An experimental study of the effect of seven bases, *J. Geophys. Res. Atmospheres*, 120,  
609 1933–1950, <https://doi.org/10.1002/2014JD022730>, 2015.
- 610 Gordon, H., Kirkby, J., Baltensperger, U., Bianchi, F., Breitenlechner, M., Curtius, J., Dias, A., Dommen, J.,  
611 Donahue, N. M., Dunne, E. M., Duplissy, J., Ehrhart, S., Flagan, R. C., Frege, C., Fuchs, C., Hansel, A.,  
612 Hoyle, C. R., Kulmala, M., Kürten, A., Lehtipalo, K., Makhmutov, V., Molteni, U., Rissanen, M. P.,  
613 Stozkhov, Y., Tröstl, J., Tsagkogeorgas, G., Wagner, R., Williamson, C., Wimmer, D., Winkler, P. M.,  
614 Yan, C., and Carslaw, K. S.: Causes and importance of new particle formation in the present-day and  
615 preindustrial atmospheres, *J. Geophys. Res. Atmospheres*, 122, 8739–8760,  
616 <https://doi.org/10.1002/2017JD026844>, 2017.
- 617 Hamed, A., Korhonen, H., Sihto, S.-L., Joutsensaari, J., Järvinen, H., Petäjä, T., Arnold, F., Nieminen, T., Kulmala,  
618 M., Smith, J. N., Lehtinen, K. E. J., and Laaksonen, A.: The role of relative humidity in continental new  
619 particle formation, *J. Geophys. Res. Atmospheres*, 116, <https://doi.org/10.1029/2010JD014186>, 2011.
- 620 Hari, P. and Kulmala, M.: Station for measuring Ecosystem-Atmosphere relations (SMEAR II), *Boreal Environ.*  
621 *Res.*, 10, 2005.
- 622 Hellmuth, O.: Columnar modelling of nucleation burst evolution in the convective boundary layer – first results  
623 from a feasibility study Part I: Modelling approach, *Atmospheric Chem. Phys.*, 6, 4175–4214,  
624 <https://doi.org/10.5194/acp-6-4175-2006>, 2006.
- 625 Huijnen, V., Williams, J., van Weele, M., van Noije, T., Krol, M., Dentener, F., Segers, A., Houweling, S., Peters,  
626 W., de Laat, J., Boersma, F., Bergamaschi, P., van Velthoven, P., Le Sager, P., Eskes, H., Alkemade, F.,  
627 Scheele, R., Nédélec, P., and Pätz, H.-W.: The global chemistry transport model TM5: description and  
628 evaluation of the tropospheric chemistry version 3.0, *Geosci. Model Dev.*, 3, 445–473,  
629 <https://doi.org/10.5194/gmd-3-445-2010>, 2010.
- 630 Jokinen, T., Sipilä, M., Junninen, H., Ehn, M., Lönn, G., Hakala, J., Petäjä, T., Mauldin, R. L. I., Kulmala, M., and  
631 Worsnop, D. R.: Atmospheric sulphuric acid and neutral cluster measurements using CI-API-TOF,  
632 *Atmospheric Chem. Phys.*, 12, 4117–4125, <https://doi.org/10.5194/acp-12-4117-2012>, 2012.
- 633 Jokinen, T., Lehtipalo, K., Thakur, R. C., Ylivinkka, I., Neitola, K., Sarnela, N., Laitinen, T., Kulmala, M., Petäjä,  
634 T., and Sipilä, M.: Measurement report: Long-term measurements of aerosol precursor concentrations in



- 635 the Finnish subarctic boreal forest, *Atmospheric Chem. Phys.*, 22, 2237–2254, [https://doi.org/10.5194/acp-](https://doi.org/10.5194/acp-22-2237-2022)  
636 [22-2237-2022](https://doi.org/10.5194/acp-22-2237-2022), 2022.
- 637 Junninen, H., Ehn, M., Petäjä, T., Luosujärvi, L., Kotiaho, T., Kostianen, R., Rohner, U., Gonin, M., Fuhrer, K.,  
638 Kulmala, M., and Worsnop, D. R.: A high-resolution mass spectrometer to measure atmospheric ion  
639 composition, *Atmospheric Meas. Tech.*, 3, 1039–1053, <https://doi.org/10.5194/amt-3-1039-2010>, 2010.
- 640 Kerminen, V.-M. and Kulmala, M.: Analytical formulae connecting the “real” and the “apparent” nucleation rate  
641 and the nuclei number concentration for atmospheric nucleation events, *J. Aerosol Sci.*, 33, 609–622,  
642 [https://doi.org/10.1016/S0021-8502\(01\)00194-X](https://doi.org/10.1016/S0021-8502(01)00194-X), 2002.
- 643 Kerminen, V.-M., Chen, X., Vakkari, V., Petäjä, T., Kulmala, M., and Bianchi, F.: Atmospheric new particle  
644 formation and growth: review of field observations, *Environ. Res. Lett.*, 13, 103003,  
645 <https://doi.org/10.1088/1748-9326/aadf3c>, 2018.
- 646 Kirkby, J., Curtius, J., Almeida, J., Dunne, E., Duplissy, J., Ehrhart, S., Franchin, A., Gagné, S., Ickes, L., Kürten,  
647 A., Kupc, A., Metzger, A., Riccobono, F., Rondo, L., Schobesberger, S., Tsagkogeorgas, G., Wimmer, D.,  
648 Amorim, A., Bianchi, F., Breitenlechner, M., David, A., Dommen, J., Downard, A., Ehn, M., Flagan, R.  
649 C., Haider, S., Hansel, A., Hauser, D., Jud, W., Junninen, H., Kreissl, F., Kvashin, A., Laaksonen, A.,  
650 Lehtipalo, K., Lima, J., Lovejoy, E. R., Makhmutov, V., Mathot, S., Mikkilä, J., Minginette, P., Mogo, S.,  
651 Nieminen, T., Onnela, A., Pereira, P., Petäjä, T., Schnitzhofer, R., Seinfeld, J. H., Sipilä, M., Stozhkov, Y.,  
652 Stratmann, F., Tomé, A., Vanhanen, J., Viisanen, Y., Vrtala, A., Wagner, P. E., Walther, H., Weingartner,  
653 E., Wex, H., Winkler, P. M., Carslaw, K. S., Worsnop, D. R., Baltensperger, U., and Kulmala, M.: Role of  
654 sulphuric acid, ammonia and galactic cosmic rays in atmospheric aerosol nucleation, *Nature*, 476, 429–  
655 433, <https://doi.org/10.1038/nature10343>, 2011.
- 656 Kleindienst, T. E.: Epoxying Isoprene Chemistry, *Science*, 325, 687–688, <https://doi.org/10.1126/science.1178324>,  
657 2009.
- 658 Kulmala, M., Maso, M. D., Mäkelä, J. M., Pirjola, L., Väkevä, M., Aalto, P., Miikkulainen, P., Hämeri, K., and  
659 O’ Dowd, C. D.: On the formation, growth and composition of nucleation mode particles, *Tellus B*, 53, 479–  
660 490, <https://doi.org/10.1034/j.1600-0889.2001.530411.x>, 2001.
- 661 Kulmala, M., Vehkamäki, H., Petäjä, T., Dal Maso, M., Lauri, A., Kerminen, V.-M., Birmili, W., and McMurry,  
662 P. H.: Formation and growth rates of ultrafine atmospheric particles: a review of observations, *J. Aerosol*  
663 *Sci.*, 35, 143–176, <https://doi.org/10.1016/j.jaerosci.2003.10.003>, 2004.





- 664 Kulmala, M., Lehtinen, K. E. J., and Laaksonen, A.: Cluster activation theory as an explanation of the linear  
665 dependence between formation rate of 3nm particles and sulphuric acid concentration, *Atmospheric Chem.*  
666 *Phys.*, 6, 787–793, <https://doi.org/10.5194/acp-6-787-2006>, 2006.
- 667 Kulmala, M., Petäjä, T., Nieminen, T., Sipilä, M., Manninen, H. E., Lehtipalo, K., Dal Maso, M., Aalto, P. P.,  
668 Junninen, H., Paasonen, P., Riipinen, I., Lehtinen, K. E. J., Laaksonen, A., and Kerminen, V.-M.:  
669 Measurement of the nucleation of atmospheric aerosol particles, *Nat. Protoc.*, 7, 1651–1667,  
670 <https://doi.org/10.1038/nprot.2012.091>, 2012.
- 671 Kulmala, M., Junninen, H., Dada, L., Salma, I., Weidinger, T., Thén, W., Vörösmarty, M., Komsaare, K.,  
672 Stolzenburg, D., Cai, R., Yan, C., Li, X., Deng, C., Jiang, J., Petäjä, T., Nieminen, T., and Kerminen, V.-  
673 M.: Quiet New Particle Formation in the Atmosphere, *Front. Environ. Sci.*, 10, 2022a.
- 674 Kulmala, M., Cai, R., Stolzenburg, D., Zhou, Y., Dada, L., Guo, Y., Yan, C., Petäjä, T., Jiang, J., and Kerminen,  
675 V.-M.: The contribution of new particle formation and subsequent growth to haze formation, *Environ. Sci.*  
676 *Atmospheres*, 2, 352–361, <https://doi.org/10.1039/D1EA00096A>, 2022b.
- 677 Kulmala, M., Cai, R., Ezhova, E., Deng, C., Stolzenburg, D., Dada, L., Guo, Y., Chao, Y., Peräkylä, O., Lintunen,  
678 A., Nieminen, T., Kokkonen, T. V., Sarnela, N., and Kerminen, T. P. & V.-M.: Direct link between the  
679 characteristics of atmospheric new particle formation and Continental Biosphere-Atmosphere-Cloud-  
680 Climate (COBACC) feedback loop, *Boreal Environ. Res.*, 28, 1–13, 2023.
- 681 Kürten, A., Rondo, L., Ehrhart, S., and Curtius, J.: Calibration of a Chemical Ionization Mass Spectrometer for the  
682 Measurement of Gaseous Sulfuric Acid, *J. Phys. Chem. A*, 116, 6375–6386,  
683 <https://doi.org/10.1021/jp212123n>, 2012.
- 684 Kyrö, E.-M., Väänänen, R., Kerminen, V.-M., Virkkula, A., Petäjä, T., Asmi, A., Dal Maso, M., Nieminen, T.,  
685 Juhola, S., Shcherbinin, A., Riipinen, I., Lehtipalo, K., Keronen, P., Aalto, P. P., Hari, P., and Kulmala,  
686 M.: Trends in new particle formation in eastern Lapland, Finland: effect of decreasing sulfur emissions  
687 from Kola Peninsula, *Atmospheric Chem. Phys.*, 14, 4383–4396, [https://doi.org/10.5194/acp-14-4383-](https://doi.org/10.5194/acp-14-4383-2014)  
688 2014, 2014.
- 689 Laarne, P., Amnell, E., Zaidan, M. A., Mikkonen, S., and Nieminen, T.: Exploring Non-Linear Dependencies in  
690 Atmospheric Data with Mutual Information, *Atmosphere*, 13, 1046,  
691 <https://doi.org/10.3390/atmos13071046>, 2022.
- 692 Lee, S.-H., Gordon, H., Yu, H., Lehtipalo, K., Haley, R., Li, Y., and Zhang, R.: New Particle Formation in the  
693 Atmosphere: From Molecular Clusters to Global Climate, *J. Geophys. Res. Atmospheres*, 124, 7098–7146,  
694 <https://doi.org/10.1029/2018JD029356>, 2019.



- 695 Lehtinen, K. E. J. and Kulmala, M.: A model for particle formation and growth in the atmosphere with molecular  
696 resolution in size, *Atmos Chem Phys*, 7, 2003.
- 697 Lehtipalo, K., Yan, C., Dada, L., Bianchi, F., Xiao, M., Wagner, R., Stolzenburg, D., Ahonen, L. R., Amorim, A.,  
698 Baccarini, A., Bauer, P. S., Baumgartner, B., Bergen, A., Bernhammer, A.-K., Breitenlechner, M., Brilke,  
699 S., Buchholz, A., Mazon, S. B., Chen, D., Chen, X., Dias, A., Dommen, J., Draper, D. C., Duplissy, J.,  
700 Ehn, M., Finkenzeller, H., Fischer, L., Frege, C., Fuchs, C., Garmash, O., Gordon, H., Hakala, J., He, X.,  
701 Heikkinen, L., Heinritzi, M., Helm, J. C., Hofbauer, V., Hoyle, C. R., Jokinen, T., Kangasluoma, J.,  
702 Kerminen, V.-M., Kim, C., Kirkby, J., Kontkanen, J., Kürten, A., Lawler, M. J., Mai, H., Mathot, S.,  
703 Mauldin, R. L., Molteni, U., Nichman, L., Nie, W., Nieminen, T., Ojdanic, A., Onnela, A., Passananti, M.,  
704 Petäjä, T., Piel, F., Pospisilova, V., Quéléver, L. L. J., Rissanen, M. P., Rose, C., Sarnela, N., Schallhart,  
705 S., Schuchmann, S., Sengupta, K., Simon, M., Sipilä, M., Tauber, C., Tomé, A., Tröstl, J., Väisänen, O.,  
706 Vogel, A. L., Volkamer, R., Wagner, A. C., Wang, M., Weitz, L., Wimmer, D., Ye, P., Ylisirniö, A., Zha,  
707 Q., Carslaw, K. S., Curtius, J., Donahue, N. M., Flagan, R. C., Hansel, A., Riipinen, I., Virtanen, A.,  
708 Winkler, P. M., Baltensperger, U., Kulmala, M., and Worsnop, D. R.: Multicomponent new particle  
709 formation from sulfuric acid, ammonia, and biogenic vapors, *Sci. Adv.*, 4, eaau5363,  
710 <https://doi.org/10.1126/sciadv.aau5363>, 2018.
- 711 Li, X., Chee, S., Hao, J., Abbatt, J. P. D., Jiang, J., and Smith, J. N.: Relative humidity effect on the formation of  
712 highly oxidized molecules and new particles during monoterpene oxidation, *Atmospheric Chem. Phys.*,  
713 19, 1555–1570, <https://doi.org/10.5194/acp-19-1555-2019>, 2019.
- 714 Liu, Q., Jia, X., Quan, J., Li, J., Li, X., Wu, Y., Chen, D., Wang, Z., and Liu, Y.: New positive feedback mechanism  
715 between boundary layer meteorology and secondary aerosol formation during severe haze events, *Sci.*  
716 *Rep.*, 8, 6095, <https://doi.org/10.1038/s41598-018-24366-3>, 2018.
- 717 Liu, Y., Yan, C., Feng, Z., Zheng, F., Fan, X., Zhang, Y., Li, C., Zhou, Y., Lin, Z., Guo, Y., Zhang, Y., Ma, L.,  
718 Zhou, W., Liu, Z., Dada, L., Dällenbach, K., Kontkanen, J., Cai, R., Chan, T., Chu, B., Du, W., Yao, L.,  
719 Wang, Y., Cai, J., Kangasluoma, J., Kokkonen, T., Kujansuu, J., Rusanen, A., Deng, C., Fu, Y., Yin, R.,  
720 Li, X., Lu, Y., Liu, Y., Lian, C., Yang, D., Wang, W., Ge, M., Wang, Y., Worsnop, D. R., Junninen, H.,  
721 He, H., Kerminen, V.-M., Zheng, J., Wang, L., Jiang, J., Petäjä, T., Bianchi, F., and Kulmala, M.:  
722 Continuous and comprehensive atmospheric observations in Beijing: a station to understand the complex  
723 urban atmospheric environment, *Big Earth Data*, 4, 295–321,  
724 <https://doi.org/10.1080/20964471.2020.1798707>, 2020.



- 725 Määttänen, A., Merikanto, J., Henschel, H., Duplissy, J., Makkonen, R., Ortega, I. K., and Vehkamäki, H.: New  
726 Parameterizations for Neutral and Ion-Induced Sulfuric Acid-Water Particle Formation in Nucleation and  
727 Kinetic Regimes, *J. Geophys. Res. Atmospheres*, 123, 1269–1296, <https://doi.org/10.1002/2017JD027429>,  
728 2018.
- 729 Marten, R., Xiao, M., Rörup, B., Wang, M., Kong, W., He, X.-C., Stolzenburg, D., Pfeifer, J., Marie, G., S. Wang,  
730 D., Scholz, W., Baccarini, A., Ping Lee, C., Amorim, A., Baalbaki, R., M. Bell, D., Bertozzi, B., Caudillo,  
731 L., Chu, B., Dada, L., Duplissy, J., Finkenzeller, H., Gonzalez Carracedo, L., Granzin, M., Hansel, A.,  
732 Heinritzi, M., Hofbauer, V., Kempainen, D., Kürten, A., Lampimäki, M., Lehtipalo, K., Makhmutov, V.,  
733 E. Manninen, H., Mentler, B., Petäjä, T., Philippov, M., Shen, J., Simon, M., Stozhkov, Y., Tomé, A.,  
734 C. Wagner, A., Wang, Y., K. Weber, S., Wu, Y., Zauner-Wieczorek, M., Curtius, J., Kulmala, M., Möhler,  
735 O., Volkamer, R., M. Winkler, P., R. Worsnop, D., Dommen, J., C. Flagan, R., Kirkby, J., M. Donahue,  
736 N., Lamkaddam, H., Baltensperger, U., and Haddad, I. E.: Survival of newly formed particles in haze  
737 conditions, *Environ. Sci. Atmospheres*, 2, 491–499, <https://doi.org/10.1039/D2EA00007E>, 2022.
- 738 Martin, S. T., Artaxo, P., Machado, L. a. T., Manzi, A. O., Souza, R. a. F., Schumacher, C., Wang, J., Andreae, M.  
739 O., Barbosa, H. M. J., Fan, J., Fisch, G., Goldstein, A. H., Guenther, A., Jimenez, J. L., Pöschl, U., Silva  
740 Dias, M. A., Smith, J. N., and Wendisch, M.: Introduction: Observations and Modeling of the Green Ocean  
741 Amazon (GoAmazon2014/5), *Atmospheric Chem. Phys.*, 16, 4785–4797, [https://doi.org/10.5194/acp-16-](https://doi.org/10.5194/acp-16-4785-2016)  
742 4785-2016, 2016.
- 743 Mauldin III, R. L., Frost, G. J., Chen, G., Tanner, D. J., Prevot, A. S. H., Davis, D. D., and Eisele, F. L.: OH  
744 measurements during the First Aerosol Characterization Experiment (ACE 1): Observations and model  
745 comparisons, *J. Geophys. Res. Atmospheres*, 103, 16713–16729, <https://doi.org/10.1029/98JD00882>,  
746 1998.
- 747 Mazon, S. B., Kontkanen, J., Manninen, H. E., Nieminen, T., Kerminen, V.-M., and Kulmala, M.: A long-term  
748 comparison of nighttime cluster events and daytime ion formation in a boreal forest, 2016.
- 749 McMurry, P. H. and Friedlander, S. K.: New particle formation in the presence of an aerosol, *Atmospheric Environ.*  
750 1967, 13, 1635–1651, [https://doi.org/10.1016/0004-6981\(79\)90322-6](https://doi.org/10.1016/0004-6981(79)90322-6), 1979.
- 751 Myers, D. C., Kim, S., Sjostedt, S., Guenther, A. B., Seco, R., Vega Bustillos, O., Tota, J., Souza, R. A. F., and  
752 Smith, J. N.: Sulfuric acid in the Amazon basin: measurements and evaluation of existing sulfuric acid  
753 proxies, *Atmospheric Chem. Phys.*, 22, 10061–10076, <https://doi.org/10.5194/acp-22-10061-2022>, 2022.



- 754 Myllys, N., Kubečka, J., Besel, V., Alfaouri, D., Olenius, T., Smith, J. N., and Passananti, M.: Role of base strength,  
755 cluster structure and charge in sulfuric-acid-driven particle formation, *Atmospheric Chem. Phys.*, 19,  
756 9753–9768, <https://doi.org/10.5194/acp-19-9753-2019>, 2019.
- 757 Neefjes, I., Laapas, M., Liu, Y., Medus, E., Miettunen, E., Ahonen, L., Quelever, L., Aalto, J., Bäck, J., Kerminen,  
758 V.-M., Lampilahti, J., Luoma, K., Mäki, M., Mammarella, I., Petäjä, T., Rätty, M., Sarnela, N., Ylivinkka,  
759 I., Hakala, S., Kulmala, M., Nieminen, T., and Lintunen, A.: 25 years of atmospheric and ecosystem  
760 measurements in a boreal forest - Seasonal variation and responses to warm and dry years, *Boreal Environ.*  
761 *Res.*, 27, 1–31, 2022.
- 762 Nieminen, T., Paasonen, P., Manninen, H. E., Sellegri, K., Kerminen, V.-M., and Kulmala, M.: Parameterization  
763 of ion-induced nucleation rates based on ambient observations, *Atmospheric Chem. Phys.*, 11, 3393–3402,  
764 <https://doi.org/10.5194/acp-11-3393-2011>, 2011.
- 765 Nieminen, T., Yli-Juuti, T., Manninen, H. E., Petäjä, T., Kerminen, V.-M., and Kulmala, M.: Technical note: New  
766 particle formation event forecasts during PEGASOS–Zeppelin Northern mission 2013 in Hyytiälä, Finland,  
767 *Atmospheric Chem. Phys.*, 15, 12385–12396, <https://doi.org/10.5194/acp-15-12385-2015>, 2015.
- 768 Nieminen, T., Kerminen, V.-M., Petäjä, T., Aalto, P. P., Arshinov, M., Asmi, E., Baltensperger, U., Beddows, D.  
769 C. S., Beukes, J. P., Collins, D., Ding, A., Harrison, R. M., Henzing, B., Hooda, R., Hu, M., Hörrak, U.,  
770 Kivekäs, N., Komsaare, K., Krejci, R., Kristensson, A., Laakso, L., Laaksonen, A., Leaitch, W. R.,  
771 Lihavainen, H., Mihalopoulos, N., Németh, Z., Nie, W., O’Dowd, C., Salma, I., Sellegri, K., Svenningsson,  
772 B., Swietlicki, E., Tunved, P., Ulevicius, V., Vakkari, V., Vana, M., Wiedensohler, A., Wu, Z., Virtanen,  
773 A., and Kulmala, M.: Global analysis of continental boundary layer new particle formation based on long-  
774 term measurements, *Atmospheric Chem. Phys.*, 18, 14737–14756, [https://doi.org/10.5194/acp-18-14737-](https://doi.org/10.5194/acp-18-14737-2018)  
775 2018, 2018.
- 776 Paasonen, P., Nieminen, T., Asmi, E., Manninen, H. E., Petäjä, T., Plass-Dülmer, C., Flentje, H., Birmili, W.,  
777 Wiedensohler, A., Hörrak, U., Metzger, A., Hamed, A., Laaksonen, A., Facchini, M. C., Kerminen, V.-M.,  
778 and Kulmala, M.: On the roles of sulphuric acid and low-volatility organic vapours in the initial steps of  
779 atmospheric new particle formation, *Atmospheric Chem. Phys.*, 10, 11223–11242,  
780 <https://doi.org/10.5194/acp-10-11223-2010>, 2010.
- 781 Paulot, F., Crouse, J. D., Kjaergaard, H. G., Kürten, A., St. Clair, J. M., Seinfeld, J. H., and Wennberg, P. O.:  
782 Unexpected Epoxide Formation in the Gas-Phase Photooxidation of Isoprene, *Science*, 325, 730–733,  
783 <https://doi.org/10.1126/science.1172910>, 2009.



- 784 Quéléver, L. L. J., Dada, L., Asmi, E., Lampilahti, J., Chan, T., Ferrara, J. E., Copes, G. E., Pérez-Fogwill, G.,  
785       Barreira, L., Aurela, M., Worsnop, D. R., Jokinen, T., and Sipilä, M.: Investigation of new particle  
786       formation mechanisms and aerosol processes at Marambio Station, Antarctic Peninsula, *Atmospheric*  
787       *Chem. Phys.*, 22, 8417–8437, <https://doi.org/10.5194/acp-22-8417-2022>, 2022.
- 788 Riccobono, F., Schobesberger, S., Scott, C. E., Dommen, J., Ortega, I. K., Rondo, L., Almeida, J., Amorim, A.,  
789       Bianchi, F., Breitenlechner, M., David, A., Downard, A., Dunne, E. M., Duplissy, J., Ehrhart, S., Flagan,  
790       R. C., Franchin, A., Hansel, A., Junninen, H., Kajos, M., Keskinen, H., Kupc, A., Kürten, A., Kvashin, A.  
791       N., Laaksonen, A., Lehtipalo, K., Makhmutov, V., Mathot, S., Nieminen, T., Onnela, A., Petäjä, T.,  
792       Praplan, A. P., Santos, F. D., Schallhart, S., Seinfeld, J. H., Sipilä, M., Spracklen, D. V., Stozhkov, Y.,  
793       Stratmann, F., Tomé, A., Tsagkogeorgas, G., Vaattovaara, P., Viisanen, Y., Vrtala, A., Wagner, P. E.,  
794       Weingartner, E., Wex, H., Wimmer, D., Carslaw, K. S., Curtius, J., Donahue, N. M., Kirkby, J., Kulmala,  
795       M., Worsnop, D. R., and Baltensperger, U.: Oxidation Products of Biogenic Emissions Contribute to  
796       Nucleation of Atmospheric Particles, *Science*, 344, 717–721, <https://doi.org/10.1126/science.1243527>,  
797       2014.
- 798 Roldin, P., Swietlicki, E., Massling, A., Kristensson, A., Löndahl, J., Eriksson, A., Pagels, J., and Gustafsson, S.:  
799       Aerosol ageing in an urban plume – implication for climate, *Atmospheric Chem. Phys.*, 11, 5897–5915,  
800       <https://doi.org/10.5194/acp-11-5897-2011>, 2011.
- 801 Ruosteenoja, K. and Räisänen, P.: Seasonal Changes in Solar Radiation and Relative Humidity in Europe in  
802       Response to Global Warming, *J. Clim.*, 26, 2467–2481, <https://doi.org/10.1175/JCLI-D-12-00007.1>, 2013.
- 803 Salma, I. and Németh, Z.: Dynamic and timing properties of new aerosol particle formation and consecutive growth  
804       events, *Atmospheric Chem. Phys.*, 19, 5835–5852, <https://doi.org/10.5194/acp-19-5835-2019>, 2019.
- 805 Salma, I., Borsós, T., Weidinger, T., Aalto, P., Hussein, T., Dal Maso, M., and Kulmala, M.: Production, growth  
806       and properties of ultrafine atmospheric aerosol particles in an urban environment, *Atmospheric Chem.*  
807       *Phys.*, 11, 1339–1353, <https://doi.org/10.5194/acp-11-1339-2011>, 2011.
- 808 Salma, I., Németh, Z., Kerminen, V.-M., Aalto, P., Nieminen, T., Weidinger, T., Molnár, Á., Imre, K., and Kulmala,  
809       M.: Regional effect on urban atmospheric nucleation, *Atmospheric Chem. Phys.*, 16, 8715–8728,  
810       <https://doi.org/10.5194/acp-16-8715-2016>, 2016.
- 811 Salma, I., Thén, W., Aalto, P., Kerminen, V.-M., Kern, A., Barcza, Z., Petäjä, T., and Kulmala, M.: Influence of  
812       vegetation on occurrence and time distributions of regional new aerosol particle formation and growth,  
813       *Atmospheric Chem. Phys.*, 21, 2861–2880, <https://doi.org/10.5194/acp-21-2861-2021>, 2021.



- 814 Sanchez, K. J., Russell, L. M., Modini, R. L., Frossard, A. A., Ahlm, L., Corrigan, C. E., Roberts, G. C., Hawkins,  
815 L. N., Schroder, J. C., Bertram, A. K., Zhao, R., Lee, A. K. Y., Lin, J. J., Nenes, A., Wang, Z., Wonaschütz,  
816 A., Sorooshian, A., Noone, K. J., Jonsson, H., Toom, D., Macdonald, A. M., Leaitch, W. R., and Seinfeld,  
817 J. H.: Meteorological and aerosol effects on marine cloud microphysical properties, *J. Geophys. Res.*  
818 *Atmospheres*, 121, 4142–4161, <https://doi.org/10.1002/2015JD024595>, 2016.
- 819 Schiro, K. A., Ahmed, F., Giangrande, S. E., and Neelin, J. D.: GoAmazon2014/5 campaign points to deep-inflow  
820 approach to deep convection across scales, *Proc. Natl. Acad. Sci.*, 115, 4577–4582,  
821 <https://doi.org/10.1073/pnas.1719842115>, 2018.
- 822 Sihto, S.-L., Kulmala, M., Kerminen, V.-M., Dal Maso, M., Petäjä, T., Riipinen, I., Korhonen, H., Arnold, F.,  
823 Janson, R., Boy, M., Laaksonen, A., and Lehtinen, K. E. J.: Atmospheric sulphuric acid and aerosol  
824 formation: implications from atmospheric measurements for nucleation and early growth mechanisms,  
825 *Atmospheric Chem. Phys.*, 6, 4079–4091, <https://doi.org/10.5194/acp-6-4079-2006>, 2006.
- 826 Spracklen, D. V., Bonn, B., and Carslaw, K. S.: Boreal forests, aerosols and the impacts on clouds and climate,  
827 *Philos. Trans. R. Soc. Math. Phys. Eng. Sci.*, 366, 4613–4626, <https://doi.org/10.1098/rsta.2008.0201>,  
828 2008.
- 829 Tunved, P., Hansson, H.-C., Kerminen, V.-M., Ström, J., Maso, M. D., Lihavainen, H., Viisanen, Y., Aalto, P. P.,  
830 Komppula, M., and Kulmala, M.: High Natural Aerosol Loading over Boreal Forests, *Science*, 312, 261–  
831 263, <https://doi.org/10.1126/science.1123052>, 2006.
- 832 Tuovinen, S., Kontkanen, J., Jiang, J., and Kulmala, M.: Investigating the effectiveness of condensation sink based  
833 on heterogeneous nucleation theory, *J. Aerosol Sci.*, 149, 105613,  
834 <https://doi.org/10.1016/j.jaerosci.2020.105613>, 2020.
- 835 Tuovinen, S., Cai, R., Kerminen, V.-M., Jiang, J., Yan, C., Kulmala, M., and Kontkanen, J.: Survival probabilities  
836 of atmospheric particles: comparison based on theory, cluster population simulations, and observations in  
837 Beijing, *Atmospheric Chem. Phys.*, 22, 15071–15091, <https://doi.org/10.5194/acp-22-15071-2022>, 2022.
- 838 Uno, I., Wang, Z., Itahashi, S., Yumimoto, K., Yamamura, Y., Yoshino, A., Takami, A., Hayasaki, M., and Kim,  
839 B.-G.: Paradigm shift in aerosol chemical composition over regions downwind of China, *Sci. Rep.*, 10,  
840 6450, <https://doi.org/10.1038/s41598-020-63592-6>, 2020.
- 841 Wang, Z. B., Hu, M., Yue, D. L., Zheng, J., Zhang, R. Y., Wiedensohler, A., Wu, Z. J., Nieminen, T., and Boy,  
842 M.: Evaluation on the role of sulfuric acid in the mechanisms of new particle formation for Beijing case,  
843 *Atmospheric Chem. Phys.*, 11, 12663–12671, <https://doi.org/10.5194/acp-11-12663-2011>, 2011.



- 844 Weber, R., Marti, J., McMURRY, P., Eisele, F., Tanner, D., and Jefferson, A.: Measured atmospheric new particle  
845 formation rates: Implications for nucleation mechanisms, *Chem. Eng. Commun. - Chem Eng Commun*,  
846 151, 53–64, <https://doi.org/10.1080/00986449608936541>, 1996.
- 847 Xu, W., Gomez-Hernandez, M., Guo, S., Secrest, J., Marrero-Ortiz, W., Zhang, A. L., and Zhang, R.: Acid-  
848 Catalyzed Reactions of Epoxides for Atmospheric Nanoparticle Growth, *J. Am. Chem. Soc.*, 136, 15477–  
849 15480, <https://doi.org/10.1021/ja508989a>, 2014.
- 850 Yan, C., Yin, R., Lu, Y., Dada, L., Yang, D., Fu, Y., Kontkanen, J., Deng, C., Garmash, O., Ruan, J., Baalbaki, R.,  
851 Schervish, M., Cai, R., Bloss, M., Chan, T., Chen, T., Chen, Q., Chen, X., Chen, Y., Chu, B., Dällenbach,  
852 K., Foreback, B., He, X., Heikkinen, L., Jokinen, T., Junninen, H., Kangasluoma, J., Kokkonen, T., Kurppa,  
853 M., Lehtipalo, K., Li, H., Li, H., Li, X., Liu, Y., Ma, Q., Paasonen, P., Rantala, P., Pileci, R. E., Rusanen,  
854 A., Sarnela, N., Simonen, P., Wang, S., Wang, W., Wang, Y., Xue, M., Yang, G., Yao, L., Zhou, Y.,  
855 Kujansuu, J., Petäjä, T., Nie, W., Ma, Y., Ge, M., He, H., Donahue, N. M., Worsnop, D. R., Kerminen, V.-  
856 M., Wang, L., Liu, Y., Zheng, J., Kulmala, M., Jiang, J., and Bianchi, F.: The Synergistic Role of Sulfuric  
857 Acid, Bases, and Oxidized Organics Governing New-Particle Formation in Beijing, *Geophys. Res. Lett.*,  
858 48, e2020GL091944, <https://doi.org/10.1029/2020GL091944>, 2021.
- 859 Yao, L., Garmash, O., Bianchi, F., Zheng, J., Yan, C., Kontkanen, J., Junninen, H., Mazon, S. B., Ehn, M.,  
860 Paasonen, P., Sipilä, M., Wang, M., Wang, X., Xiao, S., Chen, H., Lu, Y., Zhang, B., Wang, D., Fu, Q.,  
861 Geng, F., Li, L., Wang, H., Qiao, L., Yang, X., Chen, J., Kerminen, V.-M., Petäjä, T., Worsnop, D. R.,  
862 Kulmala, M., and Wang, L.: Atmospheric new particle formation from sulfuric acid and amines in a  
863 Chinese megacity, *Science*, 361, 278–281, <https://doi.org/10.1126/science.aao4839>, 2018.
- 864 Yli-Juuti, T., Riipinen, I., Aalto, P. P., Nieminen, T., Maenhaut, W., Janssens, I. A., Claeys, M., Salma, I., Ocskay,  
865 R., Hoffer, A., Imre, K., and Kulmala, M.: Characteristics of new particle formation events and cluster ions  
866 at K-pusztá, Hungary, 2009.
- 867 Zaidan, M. A., Haapasilta, V., Relan, R., Paasonen, P., Kerminen, V.-M., Junninen, H., Kulmala, M., and Foster,  
868 A. S.: Exploring non-linear associations between atmospheric new-particle formation and ambient  
869 variables: a mutual information approach, *Atmospheric Chem. Phys.*, 18, 12699–12714,  
870 <https://doi.org/10.5194/acp-18-12699-2018>, 2018.
- 871 Zhang, Y., McMurry, P. H., Yu, F., and Jacobson, M. Z.: A comparative study of nucleation parameterizations: 1.  
872 Examination and evaluation of the formulations, *J. Geophys. Res. Atmospheres*, 115,  
873 <https://doi.org/10.1029/2010JD014150>, 2010.



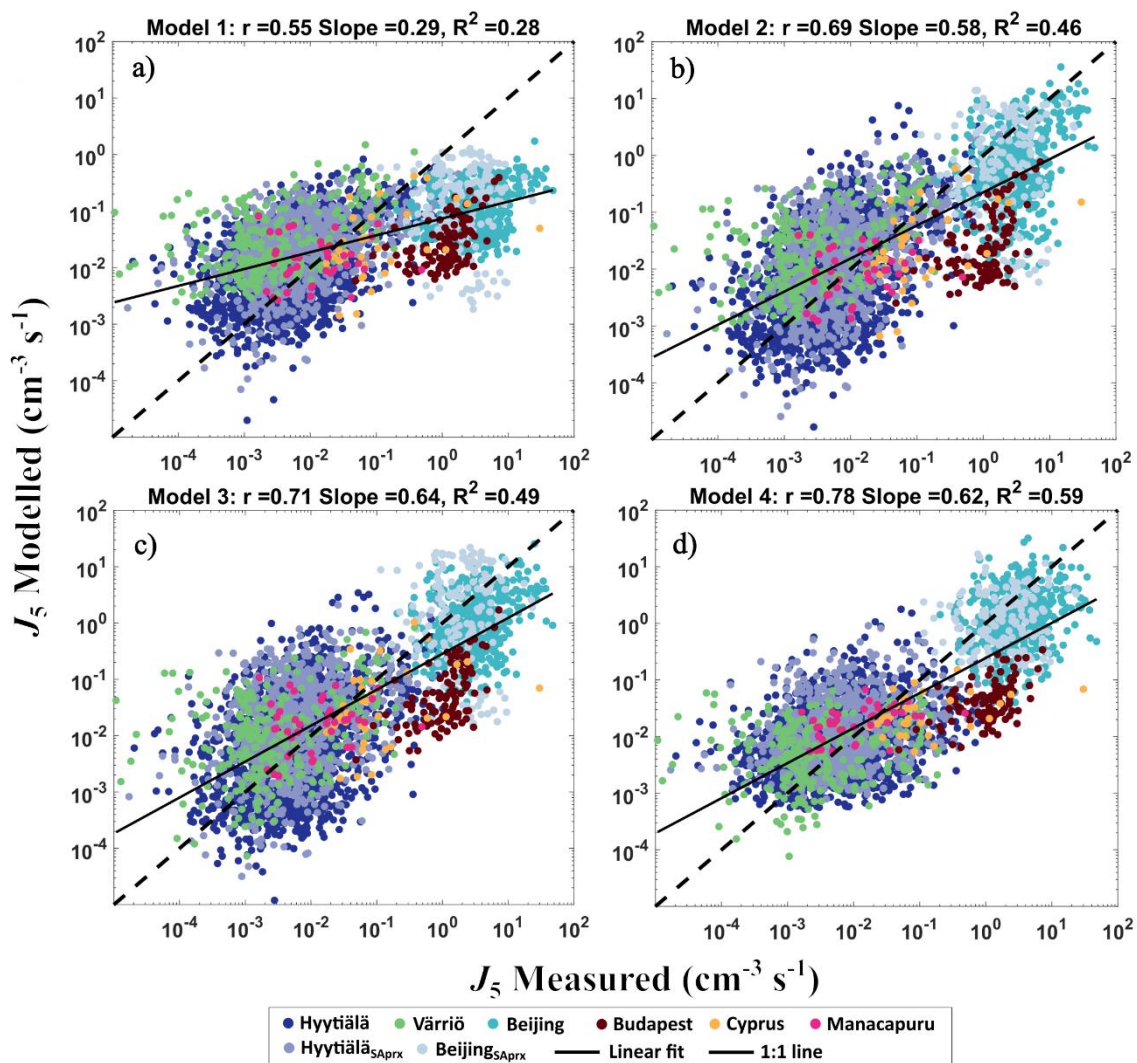
- 874 Zhao, B., Fast, J., Shrivastava, M., Donahue, N. M., Gao, Y., Shilling, J. E., Liu, Y., Zaveri, R. A., Gaudet, B.,  
875 Wang, S., Wang, J., Li, Z., and Fan, J.: Formation Process of Particles and Cloud Condensation Nuclei  
876 Over the Amazon Rainforest: The Role of Local and Remote New-Particle Formation, *Geophys. Res. Lett.*,  
877 49, e2022GL100940, <https://doi.org/10.1029/2022GL100940>, 2022.
- 878 Zhou, Y., Hakala, S., Yan, C., Gao, Y., Yao, X., Chu, B., Chan, T., Kangasluoma, J., Gani, S., Kontkanen, J.,  
879 Paasonen, P., Liu, Y., Petäjä, T., Kulmala, M., and Dada, L.: Measurement report: New particle formation  
880 characteristics at an urban and a mountain station in northern China, *Atmospheric Chem. Phys.*, 21, 17885–  
881 17906, <https://doi.org/10.5194/acp-21-17885-2021>, 2021.
- 882
- 883





884

885 Figure 1. Map of measurement locations included in this study. The number markings indicate the exact locations  
886 of the measurements. Created using a template from Canva ([www.canva.com](http://www.canva.com))

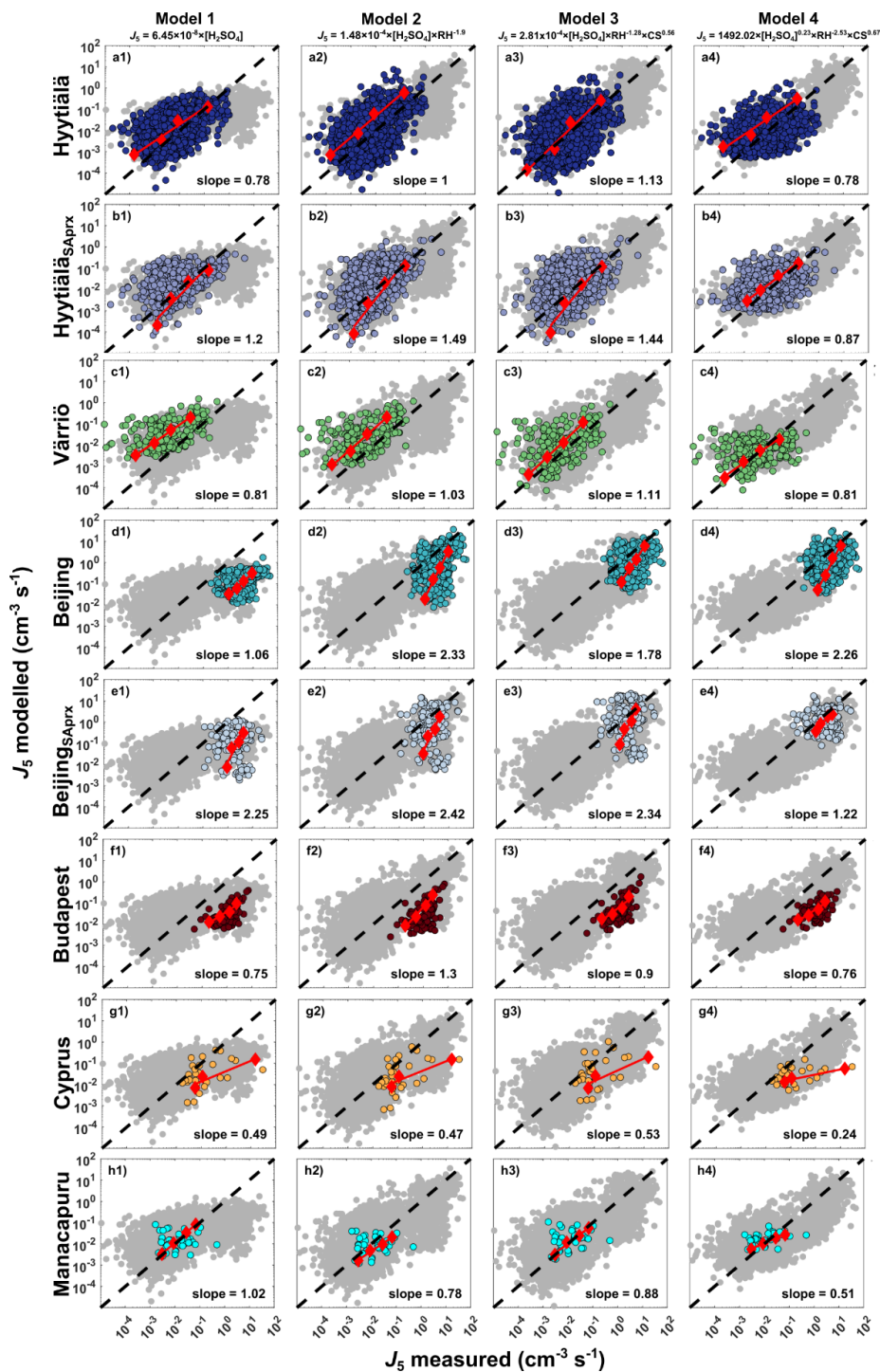


887

888 Figure 2. Modelled and measured  $J_5$  scatterplots in logscale from four models using the testing dataset containing  
889 data from all sites in hourly time resolution. Each color represents the data from one measurement site, including  
890 datasets with  $\text{H}_2\text{SO}_4$  proxy data from Hyytiälä and Beijing. The straight line showed the robust linear fit between  
891 the logscale modelled and the measure  $J_5$  values, and the dashed line represented the 1:1 line. The correlation  
892 coefficient  $r$ , slope of linear fit, and the coefficient of determination  $R^2$  are shown in the title of each subplot.

893

894



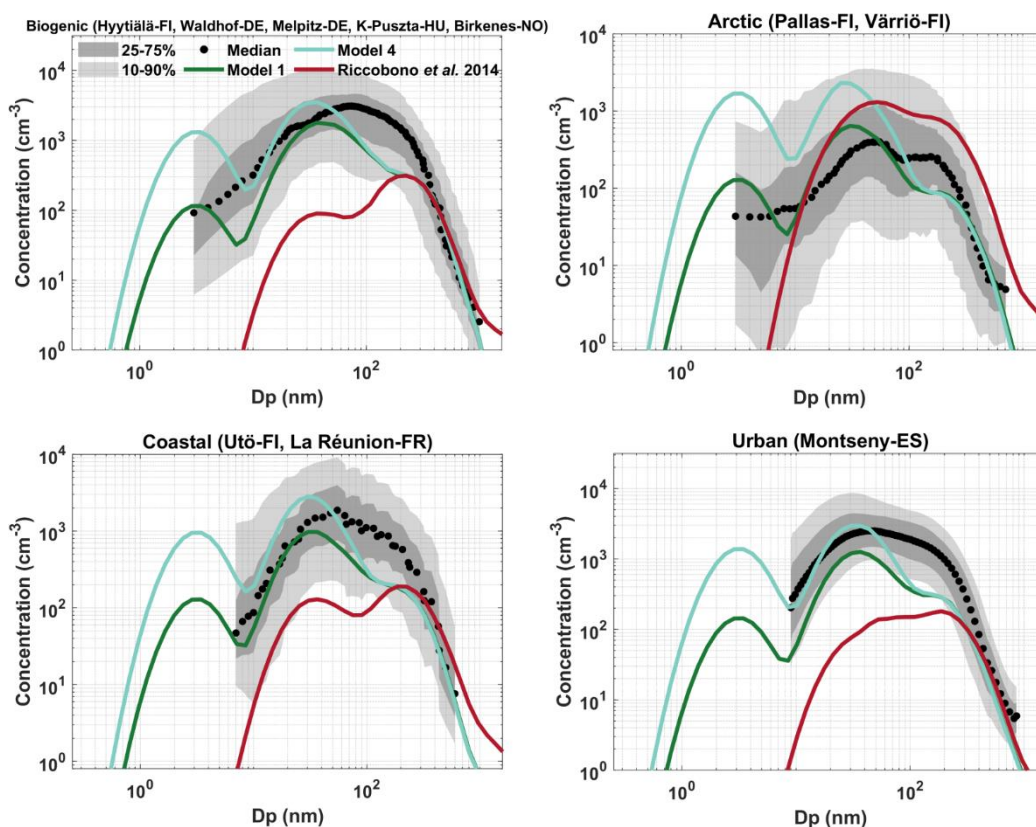
895

896 Figure 3. Modelled and measured  $J_5$  scatterplots in logscale from four models using the testing dataset containing  
 897 data from all sites in hourly time resolution. The labels on the left side of the y-axis are the site names. The



898 subscribed label “SAPrx” indicates that the input  $\text{H}_2\text{SO}_4$  concentrations was from  $\text{H}_2\text{SO}_4$  proxies. The light grey  
899 scatters are all data points from the testing dataset, the colored scatters on top of them indicate the results from the  
900 corresponding measurement site. The red diamonds are the binned daily medians to show the temporal aggregation  
901 of the model performances on daily scale data. Overall, on a daily scale presents excellent performances on model  
902 4 for boreal forest environment (a4, b4 and c4), polluted cities (d4, e4) and organic vapor dominated high humidity  
903 region (h1-h3). The red solid lines represent the linear fit on the binned hourly medians. The dashed line is the 1:1  
904 line.

905



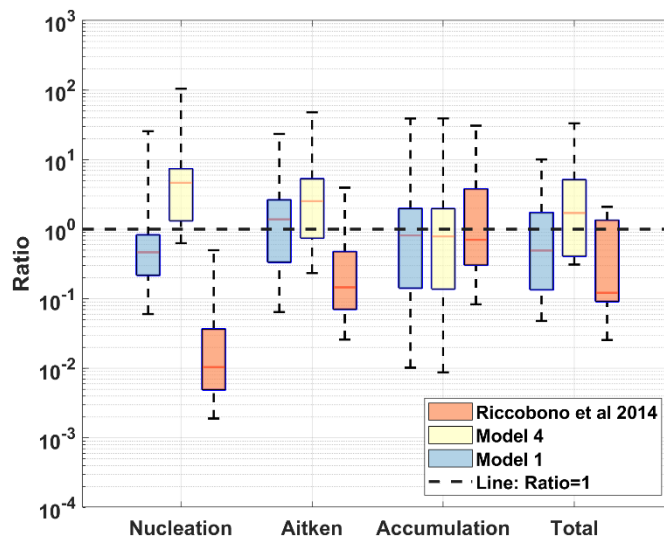
906

907 Figure 4. Environment-specific TM5-MP simulated particle number size distribution from 2018 in annual medians.  
908 Biogenic sites include rural and rural regional background environments (Hyytiälä, Waldhof, Melpitz, K-Pusztá  
909 and Birkenes); Coastal sites cover islands on the Baltic Sea and on the Indian Ocean in the southern hemisphere  
910 close to Madagascar (Utö and La Réunion); Arctic sites are two Finnish sites both situate within the Arctic Circle  
911 (Pallas and Värriö); Urban site is represented by a Spanish city Montseny.

912

913

914



915  
916 Figure 5. Ratio of simulated and measured particle number concentrations from the 14 global sites from TM5-MP  
917 simulations under three nucleation settings (Riccobono, model 1, and model 4) resulting in three particle modes  
918 (nucleation, Aitken, accumulation) in 2018 annual medians. The black line represents “ratio = 1” as a reference  
919 line. The “Total” represents the overall ratio between the simulation and the measurement particle number  
920 concentrations from all modes.

921

922



923 Table 1. Number of data points from each measurement site. The numbers in column “Total” account for the data  
 924 points from six-site combined dataset utilized in model training and testing. The training set contains 75% of the  
 925 total training data points, and 25% for testing set.

Sites	Hyytiälä	Beijing	Värriö	Budapest	Cyprus	Manacapuru	Hyytiälä <sub>proxy</sub>	Beijing <sub>proxy</sub>	Total
Training	5003	1342	728	367	140	140	-	-	7720
Testing	1642	501	248	109	34	40	797	164	3535

926  
 927 Table 2. Coefficient values ( $k_x$ ,  $k_{RH}$ ,  $k_{CS}$ ,  $k_{SA}$ ) retrieved from parameterization using training dataset. The term  $SSE$   
 928 represents the sum of squared error of each model. The units of  $k_x$  ( $x = 1, 2, 3, 4$ ) vary as the functional form of  
 929 model changes, while  $k_{RH}$ ,  $k_{CS}$ ,  $k_{SA}$  do not contain units. Since RH is counted using percentage (%), a  
 930 dimensionless number, the scaling coefficients  $k_0$  count mainly the units from  $H_2SO_4$  concentrations and CS. As  
 931 such, we must ensure that the RH input is in percentage.

Models	Functional forms	$k_x$	$k_{RH}$	$k_{CS}$	$k_{SA}$	$SSE$
1	$k_1 \times [H_2SO_4]$	$6.45E-8 (s^{-1})$				$2.78E+03$
2	$k_2 \times [H_2SO_4] \times RH^{k_{RH}}$	$1.48E-4 (s^{-1})$	-1.9			$5.16E+03$
3	$k_3 \times [H_2SO_4] \times RH^{k_{RH}} \times CS^{k_{CS}}$	$2.81E-4 ([s^{-1}]^{0.45})$	-1.28	0.56		$5.18E+03$
4	$k_4 \times [H_2SO_4]^{k_{SA}} \times RH^{k_{RH}} \times CS^{k_{CS}}$	$1492.02 ([cm^{-3}]^{0.78} \times [s^{-1}]^{0.33})$	-2.53	0.67	0.23	$3.36E+03$

932  
 933 Table 3. Summary of overall and site-specific correlation coefficients ( $r$ ) four models using the testing dataset. The  
 934 numbers in brackets under the site names represent the count for data points.

Slopes and $r$ (robust linear fit), logscale										
	Models	Hyytiälä (1642)	Beijing (501)	Värriö (248)	Budapest (109)	Cyprus (34)	Manacapuru (40)	Hyytiälä <sub>SA</sub> (797)	Beijing <sub>SA</sub> (164)	Overall
Slope	1	0.43	0.33	0.32	0.58	0.35	0.04	0.34	0.07	0.30
	2	0.62	0.57	0.40	0.66	0.48	0.15	0.57	0.23	0.58
	3	0.48	0.43	0.32	0.85	0.37	0.18	0.42	0.12	0.64
	4	0.25	0.28	0.12	0.48	0.17	0.24	0.28	0.12	0.62
$r$	1	0.43	0.30	0.44	0.54	0.42	0.04	0.41	0.004	0.55
	2	0.47	0.32	0.47	0.46	0.49	0.19	0.48	0.07	0.69
	3	0.37	0.30	0.35	0.61	0.38	0.21	0.36	0.02	0.71
	4	0.31	0.22	0.18	0.51	0.37	0.46	0.33	0.09	0.78

935  
 936  
 937